Radboud University

PHYSICS AND ASTRONOMY

BACHELOR THESIS

August 3, 2021

The phase transition of spin models coupled to dynamical triangulations

AUTHOR: Caroline Bauer

SUPERVISOR: Dr. Timothy Budd

Abstract

Dynamical triangulations are an approach to specify the integration space required to solve the quantum mechanical path integral [1]. When spin models are placed on the vertices of a dimensional dynamical triangulations, this constitutes a model of quantum gravity coupled to matter, which shows a phase transition. This thesis aims to confirm the classification of the order of the phase transition of the $q = 2, 3, 4, 5, 10$ states Potts model coupled to dynamical triangulations and thereby judge the applicability of the criteria in a random geometry setting.

The three criteria applied are the minima of Binders cumulant and the Keutosis of the magnetisation, and the value of the critical exponent ν associated with the correlation length. I could not be shown for the three criteria that they predict the classification for the Potts models as expected from matrix model calculations [2] completely correct. However, the results obtained are suffering from finite size effects and more measurements are needed to obtain more accurate estimates. To obtain final conclusions about the order of the phase transition and the applicability of the criteria, follow up research is recomended.

Contents

1 Introduction

Einsteins classical theory of general relativity is expected to break down down at small length scales, due to increasing quantum fluctuations [1]. To still be able to describe the gravitational force on scales near the Planck length, quantum gravitation aims to find a theory that includes these fluctuations. Inspiration for such a theory can for example be found in the path integral formalism of quantum mechanics as formulated by Richard Feynman [3]. There, to evaluate the integral the path of a particle is first discretised into piecewise linear parts. Then, the number of pieces is taken to infinity and the original path is recovered. Similarly, quantum gravity may be approached via a path integral over all possible space time geometries weighted by the Einstein-Hilbert action. To be able to carry out the integral and thus perform explicit calculations, the space over which integral is carried out must be specified [1].

An attempt to specify this integration space is via the theory of dynamcial triangulations. Dynamical triangulations are obtained by gluing polygons together at their edges. More specifically, only polygons with a given edge length a are allowed. Therefore, two dimensional triangulations are build only out of equilateral triangles. Depending on how many triangles meet each other at a vertex after gluing, the resulting piece of space can have positive, negative or no curvature [3]. By allowing the connectivity of the triangles to change, all possible space time geometries can be recovered. Although, no predictions that are empirically testable have resulted from the theory of dynamical triangulations yet [1], the two dimensional case serves as a toy model to develop and test tools necessary to study different discretisations of the integration space [3], as e.g. causal dynamical triangulations, or higher dimensional cases.

In general, discretised building blocks of space time, as for example the triangles in dynamical triangulations, have no fundamental nature, they are merely mathematical tools. Therefore, a theory for quantum gravitation should be invariant upon rescaling these building blocks. In other words, the geometries used to formulate the discretised version of the path integral should be scale invariant.

Scale invariance can for example be found in the vicinity of the phase transition of the Ising model, which is a simple statistical toy model of a magnet. Figure (1) shows snapshot of the two dimensional Ising model on a square lattice at the critical point, which all have been taken at different length scales. Judging by eye, the scales cannot be distinguished. Upon the phase transition the Ising model shows scale invariance, which is a shared feature among all continuous phase transitions [5]. Keeping this property in mind, quantum gravity research is interested in the phase transition of various statistical models that involve triangulations, as they are, when showing a continuous phase transition, a possible candidate for a scale invariant geometry and thus integration space.

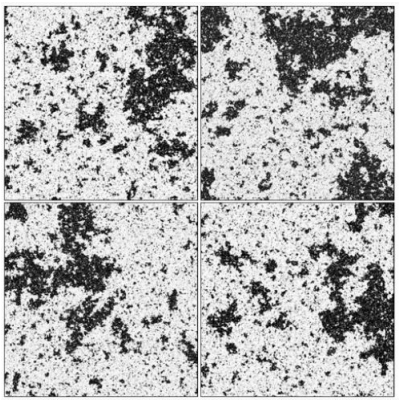

Figure 1: Snapshots of the two dimensional Ising model on a square lattice at the critical point taken at different length scales by D. Ashton [4].

Dynamical triangulations can be coupled to matter to study the influence space has on matter and the other way around [3]. In practice, this may be done by coupling Ising spins to the vertices of a dynamical triangulation. Such a statistical system can be generalised to Potts models that allow q different spins states instead of two. Based on matrix models calculations, it has been suggested that the phase transition of the Potts model coupled to a triangulation is continuous for $q \leq 4$ and discontinuous for all higher values of q [2].

Literature provides criteria to classify the order of a phase transition, which can be applied to empirical data of a statistical system obtained by a Monte Carlo simulation. The criteria are formulated in a setting where the lattice is static. In random geometry settings, the lattice may be dynamical, as for example in the case of the Potts model coupled to a triangulation. The criteria thus may not trivially apply to such a setting as well [6].

This thesis aims to confirm the classification of the phase transition of a $q = 2,3,4,5$ and $q = 10$ states Potts model coupled to a dynamical triangulation. From this point of view, three criteria for the classification of phase transitions will be reviewed to answer the question:
'To which extent can the (finite-size scaling) criteria for the order of phase transitions on flat space (regular lattice) be applied to spin models coupled to dynamical triangulations?'.

2 Definition of the models

2.1 The two dimensional Ising model

The two dimensional Ising model on a square lattice is one of the simplest statistical models that shows a phase transition. The analytical solution as well as numerical methods are well studied, hence it often serves as a toy model. The Ising model is described by the Hamiltonian H, given by

$$H = -J \sum_{\langle i,j \rangle} s_i s_j - B \sum_i s_i \tag{1}$$

, where J is the spin coupling constant, s_i the spin of the i-th site on the lattice and the sum is performed over all neighbouring spin pairs i and j. The second term describes the energy contribution of an external magnetic field B, if present. For this project the magnetic field is chosen to be zero. The spins s_i can take the values ± 1, hence can point either up or down, as depicted in figure (2). Depending on the value of the coupling constant J, the Ising model can either describe a ferromagnet or an anti-ferromagnet. If $J > 0$, aligned spins lower the energy due to the minus sign, hence the system behaves like a **ferromagnet**, where spins tend to align with each other. If $J < 0$, the opposite is the case. Anti aligned spins lower the energy, and the system behaves like an **anti-ferromagnet**.

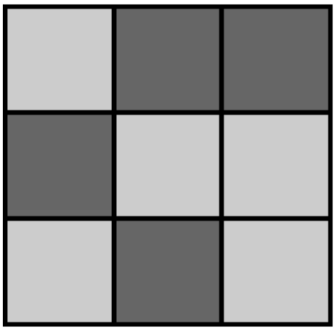

Figure 2: Schematic depiction of a three by three Ising model. Dark grey squares indicate an up and light grey squares a down spin.

The partition function of the Ising model [7] for a magnetic field $B = 0$ reads

$$Z = \sum_{\{s_i\}} e^{-\beta J \sum_{\langle i,j \rangle} s_i s_j} \tag{2}$$

, where the sum is carried out over all possible spin configurations $\{s_i\}$.

When increasing the temperature T of the system, the behaviour of the spins changes, as more thermal energy is available to overcome the energy needed to flip a spin to the opposite orientation. This change can be measured by a so called **order parameter**, as for example the average magnetisation $\langle M \rangle$, defined as

$$\langle M \rangle = \left\langle \sum_i s_i \right\rangle \tag{3}$$

, where we sum over all spin values s_i on the lattice. The average magnetisation (from now on often referred to as magnetisation) obtained from a simulation of the Ising model is plotted in figure (3). It can be observed, that the magnetisation drops from its maximal value to zero at about $T_c \approx 2.3$. This temperature is called the **critical temperature**, and marks the temperature, at which the macroscopic properties, here the magnetisation, of the system change drastically. There, a **phase transition** is happening. Below the critical temperature, for $T < T_c$, the system is in its **ferromagnetic phase**, where spins tend to align and the magnetisation is maximal; for $T > T_c$ it is in a **paramagnetic phase**, where spins tend to anti-align and the magnetisation is zero.

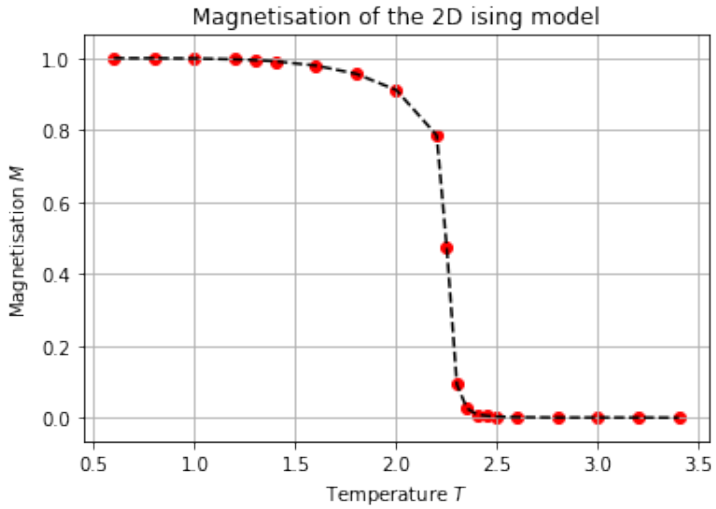

Figure 3: The average magnetisation of a 10 × 10 two dimensional Ising model as a function of temperature, simulated with the Metropolis algorithm, which will be introduced in section (3.3)*. The magnetisation is normalised by its maximal value, which it takes at the lowest temperature measured, here* $T = 0.5$.

2.2 Potts models on a square lattice

The q-states Potts model [7] is equivalent to the Ising model, but allows q different spin states instead of two. Its Hamiltonian is given by

$$H = -J \sum_{\langle i,j \rangle} \delta_{s_i,s_j} \tag{4}$$

, where the sum is carried out over all nearest neighbour spin pairs i and j. δ_{s_i,s_j} is the Kronecker delta defined as:

$$\delta_{s_i,s_j} = \begin{cases} 1 & \text{if } s_i = s_j \\ 0 & \text{if } s_i \neq s_j \end{cases} \tag{5}$$

As for the Ising model, neighbouring spins tend to align if the coupling constant J is positive, and anti-align if J is negative.

The 2-state Potts model is equivalent to the Ising model, which can be seen by adding and subtracting $\frac{1}{2}\sum_{\langle i,j \rangle} J$ to the Hamiltonian H [7]:

$$H = -\frac{1}{2} J \sum_{\langle i,j \rangle} 2\left(\delta_{s_i,s_j} - \frac{1}{2}\right) - \frac{1}{2} \sum_{\langle i,j \rangle} J \tag{6}$$

Then, the term in brackets satisfies:

$$2\left(\delta_{s_i,s_j} - \frac{1}{2}\right) = \begin{cases} 1 & \text{if } s_i = s_j \\ -1 & \text{if } s_i \neq s_j \end{cases} \tag{7}$$

Thus, for the 2-states Potts model the Hamiltonian is equivalent to the Hamiltonian of the Ising model defined in equation (1) with zero magnetic field up to a re-scaling of the coupling constant J by a factor two and an additive constant.

Magnetisation of the Potts model

Allowing more than two spin states in the Potts models, there are q equivalent ground state configurations in the low temperature range, namely those where all spins take one of the q possible values. All ground states should be treated on a similar footing, as they are equal in energy. However, when just summing over all spins and then averaging over time, as we did for the magnetisation of the Ising model in (3), the resulting magnetisation e.g. at low temperature would differ from one, as the spin values $q_i = 1, 2, ...q$ introduce a different weighting for the ground states.

A possible solution to this issue is to consider the magnetisation of the Potts model as a complex vector [8] rather than a real integer. A spin s_j is then associated with a complex vector with unit length, and the polar angle ϕ_j that the vector includes with the x axis, which entails the information in which of the q possible states the spin s_j is in.

Mathematically expressed, the polar angle ϕ_j takes the values:

$$\phi_j = \frac{2\pi j}{q}, \qquad j \in 1, 2, ..., q \tag{8}$$

To calculate the total average magnetisation across the lattice one then needs to sum over the complex magnetisation of all N spins.

$$M = \frac{1}{N} \sum_{j=1}^{N} e^{i\phi_j} \tag{9}$$

The value of the sum is then normalised by the total number of spins N on the lattice to obtain a maximal magnetisation of one at minimal temperature.

Equation (9) can be rewritten using Euler's equation

$$M = |M| \left(\cos(\phi) + i \sin(\phi)\right) \tag{10}$$

, where $|M|$ denotes the absolute value of the average magnetisation and ϕ the polar angle of the total spin state across the lattice. The angle ϕ therefore estimates, which value of q is the most present.

2.3 Dynamical triangulations coupled to matter

Triangulations aim to discretize Riemannian geometry [9], and form the basis of a possible theory for quantum gravitation. A triangulation can be obtained by cutting a piece of paper into polygons and gluing them together at their edges, as illustrated in figure (4). In this thesis, only triangulations consisting out of equilateral triangles are considered, which represents a model of two dimensional quantum gravity.

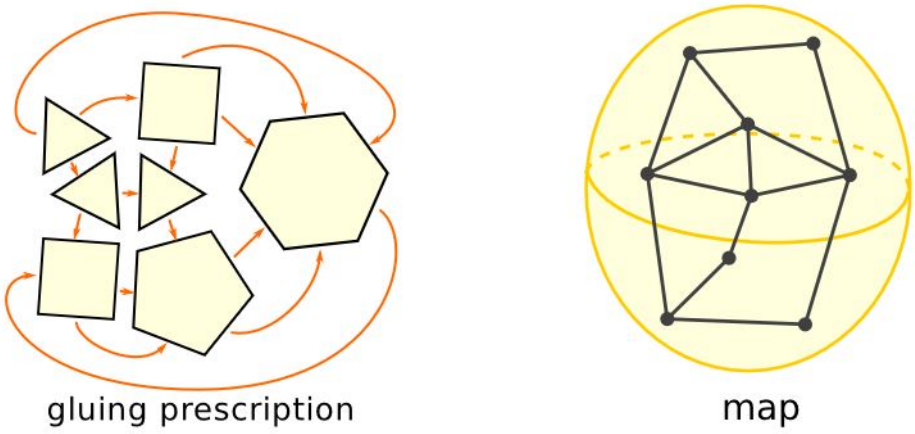

Figure 4: A triangulation can be described by determining which half edges of a bunch of polygons have been glued together. This results in a gluing prescription and an embedding in a surface. Illustration by T.Budd [9].

Triangulations may be changed either by adjusting the shape of the polygons, or by influencing the way the polygons are connected (glued together). Regge calculus is the field concerned with the former adjustments. The latter results in so called **dynamical triangulations**, which is what will be considered in this thesis.

The partition function of a dynamical triangulation is formulated [9] as

$$Z_{DT}(N) = \sum_{T} 1 \tag{11}$$

, where the sum is carried out over all triangulations T with N edges.

A **combinatorial map** [9] is a convenient way to encode a triangulation, in particular when working with computer simulations. It describes how the polygons are glued together and provides a way to navigate across the triangulation.

Each polygon consists of edges, which are labelled by integers. When gluing the polygons together, two edges meet each other. These two edges are from now on called half-edges, as each of them forms half of the new edge created.

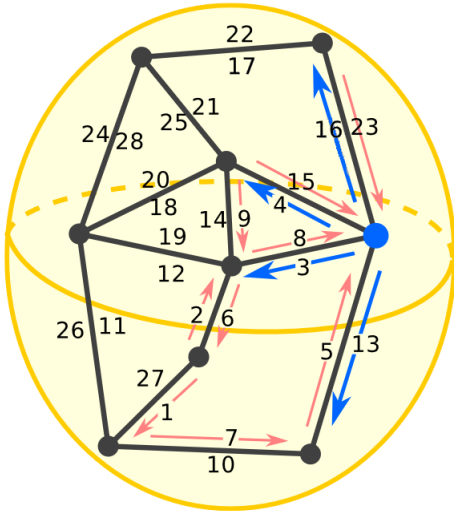

Figure 5: A visualisation of the combinatorial map on a triangulation by T. Budd. Each half edge is labelled with an integer, the orientation of the half edges (orange arrows) is counterclockwise in each face. Vertices are associated with the half edges pointing away from that vertex [9].

The way in which the polygons are glued together is described with the permutations n and a on the edge labels $\{1,2,...,N\}$, standing for next and adjacent respectively. Both permutations take a half-edge label integer as input and return the corresponding next (counterclockwise) or adjacent half edge. For example, in figure (5) the next permutation returns

$$n(3) = 6, \qquad n(7) = 5 \tag{12}$$

, and the adjacent permutation gives:

$$a(3) = 8, \qquad a(7) = 10 \tag{13}$$

A face of the triangulation can be associated with the cycles of the next permutation, for example:

$$n = (3\ \ 6\ \ 1\ \ 7\ \ 5)(2\ \ 12\ \ 11\ \ 27)\text{..} \tag{14}$$

Hence, applying the next permutation one will always stay within the same phase until returning back to the half edge one started with.

Edges of the triangulation are associated with two adjacent half edges, which are represented by the cycles of the adjacent permutation, as e.g.:

$$a = (2\ \ 6)(3\ \ 8)..\tag{15}$$

Thus, the adjacent permutation can be used to change the face, and its order is always two.

The vertices of the triangulation can be identified with the cycles of the combined permutation $n \circ a$, that first gives the adjacent and then the next half- edge of the input label. The cycles contain all the half-edges with an orientation away from the vertex, for example:

$$n \circ a = (3\ \ 4\ \ 16\ \ 13)...\tag{16}$$

The order of a cycle equals the degree of the corresponding vertex, which measures the number of half edges that depart from this vertex.

Spins coupled to a dynamical triangulation

When Ising spins are coupled to dynamical triangulations, this represents a model of two dimensional quantum gravity coupled to a matter field. One can choose to place the spins in the middle of each triangle, or on the vertices. In this thesis it is chosen to couple the spins to the vertices (see figure (6)), as this is the less studied case in literature.

The full partition function of two dimensional quantum gravity coupled to matter reads

$$Z_{\text{DT+Ising}} = \sum_T Z_{\text{Ising}}(T) = \sum_T e^{\beta H(T,\{s_i\})}\tag{17}$$

, where the sum is again carried out over all triangulations T with N edges, and H denotes the Hamiltonian of the Ising model on the triangulation T with spin configuration $\{s_i\}$.

Similarly, also the Potts model can be coupled to a dynamical triangulation. The only difference is that there are more possible spin states per site.

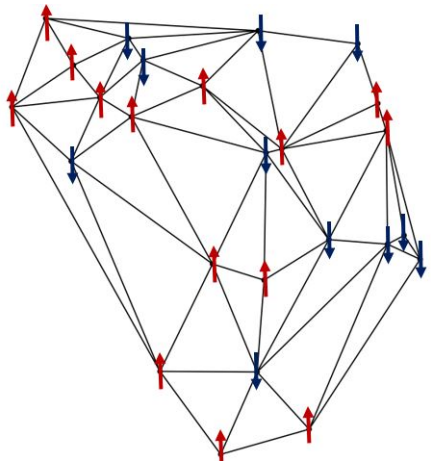

Figure 6: Schematic depiction of a triangulation with up (red) and down (blue) spins coupled to the vertices [10].

3 Monte Carlo simulations

In this section the Monte Carlo techniques necessary to simulate the models defined in section (2) are introduced after a short general introduction.

3.1 Introduction to Monte Carlo simulations

Classical statistical mechanics defines the **canonical ensemble** as a system that exchanges energy with an infinite heat bath in thermal equilibrium. Each state μ of the small system is associated with an energy E_μ, which determines the probability p_μ[11] for the system to be in this state as

$$p_\mu = \frac{1}{Z} e^{-\beta E_\mu} \tag{18}$$

, where Z is the partition function and the inverse temperature β is defined as:

$$\beta = \frac{1}{k_B T} = \frac{1}{T} \tag{19}$$

The Boltzmann constant k_B is considered in natural units to be equal to one.

The kind of Monte Carlo simulations [7] of interest for this thesis is designed such that in equilibrium it samples states from the **Maxwell Boltzmann statistics** introduced in (18). To phrase it differently, the states which the system passes through over time occur with a probability p_μ, which is equal to the Boltzmann probability.

To ensure this equilibrium condition, a so called **Markov process** is used, which produces a time sequence of random states of the system. The probability distribution with which the states occur in the time sequence approaches the Boltzmann distribution after an equilibration time. The resulting series of states is called a **Markov chain**. Convenient criteria to ensure that a Markov process samples states from the correct distribution are ergodicity and detailed balance.

The requirement of **ergodicity** states that it must be possible to reach every state of the system from any other state. An ergodic algorithm does not have limit cycles and therefore ensures that a stable equilibrium can be reached.

Detailed balance imposes a condition on the transition probabilities: the probability for the system to be in a state μ and then transition to an other state ν must be equal to the probability of finding the system in the state ν and then transition to μ. This condition resembles the time reversible symmetry present in classical statistical systems. Mathematically, detailed balance is formulated as

$$p_\mu P(\mu \to \nu) = p_\nu P(\nu \to \mu) \tag{20}$$

, where p_μ and p_ν are the probabilities to find the system in state μ and ν respectively. When reordering equation (20) and substituting the Boltzmann probabilities according to (18), the following condition for the transition probabilities is found

$$\frac{p_\mu}{p_\nu} = \frac{P(\nu \to \mu)}{P(\mu \to \nu)} \stackrel{!}{=} \exp(\beta(E_\nu - E_\mu)) \tag{21}$$

, which relates the transition probabilities to the energies E_ν and E_μ of the respective states.

If a Markov process satisfies both ergodicity and detailed balance, the equilibrium distribution is indeed the Boltzmann distribution.

3.2 The Metropolis algorithm

The goal of this section is to develop an algorithm to simulate the thermal fluctuations of the two dimensional Ising model on a square lattice, which can be a time consuming computational task [7]. The number of states is given by 2^N, where N is the number of spins in the system. A 10×10 Ising model has already $2^{100} \approx 1.3 \cdot 10^{30}$ different states, implying that there are about 10^{30} different choices for the next state in the Markov chain at every iteration. Additionally, the goal is to study the system in the thermodynamic limit where $N \to \infty$, as only in this limit the notion of phase transitions is well-defined [11]. Thus, to obtain a satisfactory estimate, we must be able to simulate as large system sizes as possible and require an algorithm that simplifies the situation enough to do so in a reasonable about of time.

One of the commonly used algorithms is the **Metropolis algorithm** [7], which is based on the principles of Monte Carlo simulation explained above. We will consider the case where the magnetic field B is zero, and assume that spins on opposite sites of the square lattice are connected by periodic boundary conditions.

The Metropolis algorithm relies on a so called **single spin flip dynamics**, meaning that at each iteration there is maximally one spin flipped compared to the previous state. This lowers the number of possible states for the next iteration from $2^N - 1$ to N. Every algorithm that flips with a non-zero probability automatically satisfies the principle of ergodicity, as given a certain state, every other configuration of the system can be reached by flipping each individual spin to point in the desired direction.

To satisfy detailed balance, the transition probabilities must satisfy equation (20). To simplify the situation, the transition probability from a state μ to a state ν is split into a product of a selection probability g and an acceptance ratio A.

$$P(\mu \to \nu) = g(\mu \to \nu) A(\mu \to \nu) \tag{22}$$

Applying equation (22), the condition for detailed balance reads:

$$\frac{p_\mu}{p_\nu} = \frac{P(\nu \to \mu)}{P(\mu \to \nu)} = \frac{g(\nu \to \mu) A(\nu \to \mu)}{g(\mu \to \nu) A(\mu \to \nu)} \stackrel{!}{=} \exp(\beta(E_\nu - E_\mu)) \tag{23}$$

By choosing appropriate selection probabilities and acceptance ratios, this condition can be satisfied, it would be ensured that the equilibrium distribution is indeed the Boltzmann distribution.

One possible choice for the probabilities g and A result in the following recipe for the Metropolis algorithm:

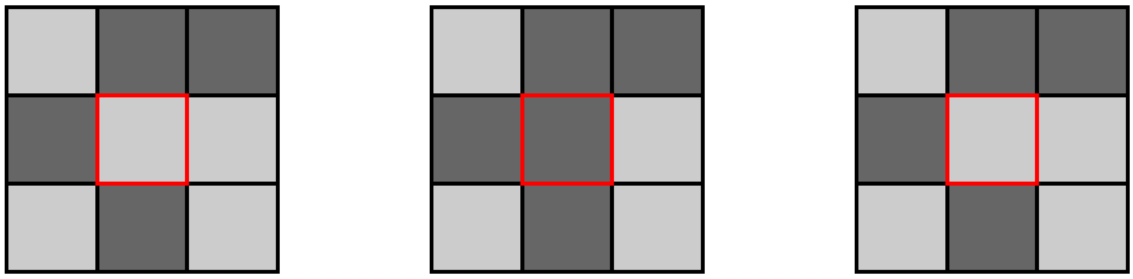

(a) *(b)* *(c)*

Figure 7: Schematic depiction of a 3×3 *Ising model, where the dark grey squares represent the* $s = 1$ *state and the light grey squares the* $s = -1$ *state. (a) A random spin in of the state* μ *is selected, which is (b) accepted and flipped to form the state* ν*, or (c) rejected and not flipped and thus remains in* μ*.*

1. Select a spin randomly, see figure (7a), with probability

$$g(\mu \to \nu) = \frac{1}{N} \tag{24}$$

, where N is the total number of spins on the 2D lattice and ν is one of the N states that is obtained by flipping exactly one spin in the state μ. The simulation is thus equally likely to start at any one of the spins on the lattice. Note, that by choosing the selection probability **independent** of the state the system is in, the condition of detailed balance in equation (23) simplifies to:

$$\frac{A(\nu \to \mu)}{A(\mu \to \nu)} \stackrel{!}{=} \exp(\beta(E_\nu - E_\mu)) \tag{25}$$

2. Accept the flip with probability

$$A(\mu \to \nu) = \begin{cases} \exp\left(-\beta(E_\nu - E_\mu)\right) & E_\nu - E_\mu > 0 \\ 1 & \text{else} \end{cases} \tag{26}$$

, which satisfies equation (25). If $E_\nu > E_\mu$, the probability $A(\nu \to \mu)$ is equal to the exponential and $A(\mu \to \nu)$ is equal to one and the condition is satisfied. A similar argument holds for $E_\nu < E_\mu$. If $E_\nu = E_\mu$ both transition probabilities are equal to one, as is the exponent on the right hand side of equation (25). In practice, the energy of the initial configuration and of the one obtained when flipping the spin selected in step one are compared. Would it be an energy loss, the flip is always accepted (see figure (7b)). If it results in an energy gain, the flip is accepted with the exponential probability, and the selected spin remains unchanged, as shown in figure (7c).

3. Repeat

Equipped with this algorithm, the thermal fluctuations of the Ising model can be simulated as a function of temperature to, for example, measure the magnetisation as in figure (3).

3.3 The Wolff algorithm

The Metropolis algorithm has a bottleneck, the so- called **critical slowing down** [7], which becomes especially important if one attempts to apply it to systems with a large number of spins N.

To understand why the algorithm slows down we have to introduce the so called **correlation length** [7]. When flipping a spin on the lattice, the correlation length measures how far away from this spin other spins still feel the influence of the flip. Near the phase transition of the Ising model in the thermodynamic limit this length diverges. This results in the tendency of neighbouring spins to align and magnetic domains form. In section (4.4), we will see that the divergence of the correlation length is actually a shared property amongst all systems that have the same type of phase transition as the Ising model.

Suppose during the first step of the Metropolis algorithm, a spin inside such a domain is selected. All its neighbours point in the same direction, flipping the spin causes a maximal energy gain and the acceptance probability for this move is low. Thus, the flip is very likely to be rejected. As many domains form in the critical region around T_c, the algorithm spends most of the time rejecting moves, thus contributing nothing to the measurements. Therefore, the metropolis algorithm slows down in the vicinity of the phase transition.

To improve this bottleneck of the Metropolis algorithm the Wolff algorithm [7] can be used . Recall that the Metropolis algorithm relied on single spin flip dynamics, which was causing the algorithm to slow down near the phase transition. The Wolff algorithm is a **cluster algorithm** and attempts to flip a whole bunch of spins, pointing all in the same direction, at the same time and by this speeds up the simulation.

The following list shows a recipe for the Wolff algorithm:

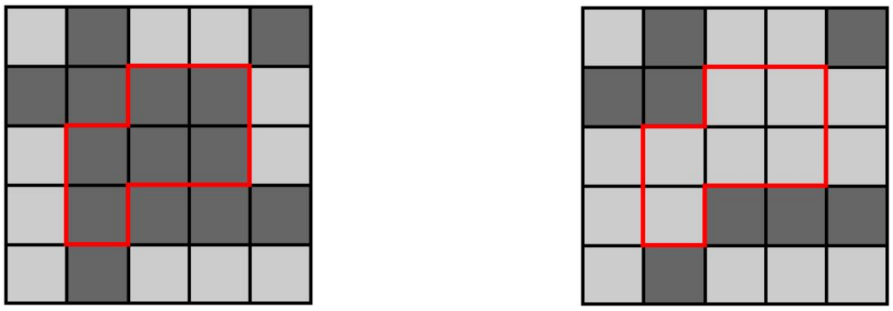

(a) *(b)*

Figure 8: Illustration of the Wolff algorithm for the 2D Ising model. A seed spin is selected, and a cluster is built around it (a), which is then flipped (b) as a whole.

1. Select a spin with uniform probability across the lattice
2. Add its nearest neighbours to the cluster with a temperature dependent probability P_{add} , if it points in the same direction. If the neighbouring spin points in the opposite direction do not add it to the cluster.
3. Repeat step two for the spins at the new boundary until all neighbours have either the wrong spin or have been rejected.
4. Flip the whole cluster.

We will see that for the Algorithm the acceptance probability A for each move is maximal and equal to one, while the selection probability is more complex. To motivate our choice for the probabilities, we again have to look closer at the condition of detailed balance as formulated in equation (20).

Let us first clarify some terminology [7]: All aligned neighbours are said to have a **bond** between them, whereas anti-aligned neighbours are **anti-bonded**.

Suppose μ is a state of the Ising model and when one cluster is flipped the state ν is obtained. Assume that, in the state μ, there are $n+m$ neighbouring spin pairs at the boundary, of which each one spin is inside the cluster and one is outside; n denotes the number of bonded pairs and m the number of anti-bonded pairs, as shown in figure (9a).

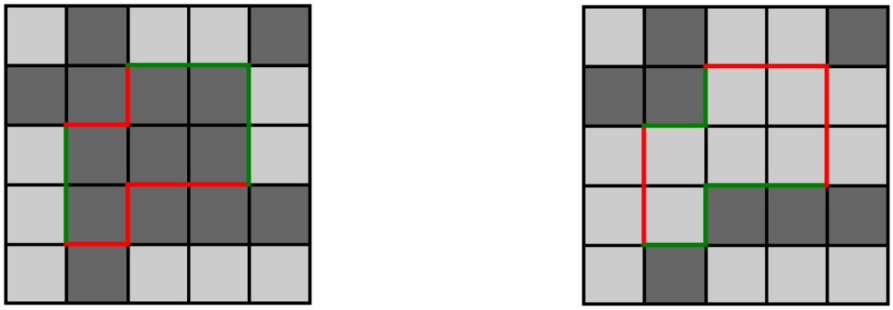

(a) *(b)*

Figure 9: The Ising model in (a) a state μ with n bonds (red) and m anti-bonds (green) at the clusters boundary and in (b) a state ν which is obtained by flipping the cluster. By doing to, the bonds become anti- bonds and vice versa.

The selection probability $g(\mu \to \nu)$ [7] for the cluster that lets the system transition from state μ to state ν depends not only on the number of spins, which have been added to the cluster, but also on those which have been rejected, and hence are situated just outside the boundary.

The probability to not add a spin with an opposite value as the seed spin to the cluster is one, but to not add a spin with the same value is given by $1-P_{\text{add}}$. An anti-bond at the boundary implies the first scenario, while a bond can only be caused by the second. If there are in total $n+m$ spins at the clusters boundary, the selection probability scales with $g(\mu \to \nu) \propto 1^m(1-P_{\text{add}})^n = (1-P_{\text{add}})^n$. The proportionality constant is given by the probability P_{add} to the power of the size of the cluster.

Due to ergodicity, there is also a move taking the system back from state ν to μ. During this move, there are then m bonded spins at the clusters boundary and the selection probability reads $g(\nu \to \mu) \propto (1-P_{\text{add}})^m$.

Thus, the condition for detailed balance can be written according to equation (20)

$$\frac{g(\nu \to \mu)A(\nu \to \mu)}{g(\mu \to \nu)A(\mu \to \nu)} = \frac{(1-P_{\text{add}})^n}{(1-P_{\text{add}})^m}\frac{A(\nu \to \mu)}{A(\mu \to \nu)} \stackrel{!}{=} \exp\big(\beta(E_\nu - E_\mu)\big) \tag{27}$$

, where the proportionality constants has been cancelled out, because in the forward and backward move the size of the cluster is the same.

Next, we will evaluate the right hand side of equation (27). The energy of a given spin configuration is calculated by performing a sum over all pairs of nearest neighbours, as defined by the Hamiltonian in equation (1).

The energy contribution of two neighbouring spins does thereby not depend directly on their value, but rather on their respective orientation to on another. Bonded spins contribute an energy $-J$, whereas the anti-bonded pairs contribute $+J$. To calculate the energy difference $E_\nu - E_\mu$, expand E_ν as

$$E_\nu = E + E_b(\nu) + C \tag{28}$$

, where E is the energy contributed by all the bonds inside the cluster, E_b the contribution of the bonds and anti-bonds at the clusters boundary, and C is the energy of all the bonds and anti-bonds, which are not part of the cluster, nor its boundary. Then, the energy difference between the states ν and μ is

$$E_\nu - E_\mu = E_b(\nu) - E_b(\mu) \equiv \Delta E_b \tag{29}$$

where the contribution E and C of the bonds inside and outside the cluster cancel, as they remain unchanged during the move. The only contribution that does change is caused by the bonds at the clusters boundary. If a bond is broken upon a flip, this increases the energy by 2J, if a bond is created, the energy is lowered by -2J. Hence ΔE_b is given by the number of bonds made minus the number of bonds broken. Going from μ to ν, there are n bonds broken, and m bonds made, hence $\Delta E_\mathrm{b} = 2J \cdot (m-n)$.

The expression for ΔE combined with equation (27) and then rewritten results in the condition:

$$\frac{A(\nu \to \mu)}{A(\mu \to \nu)} = \left(e^{2\beta J}(1 - P_\mathrm{add})\right)^{m-n} \tag{30}$$

Now consider choosing

$$P_\mathrm{add} = 1 - e^{-2\beta J} \tag{31}$$

, then equation (32) reads

$$\frac{A(\nu \to \mu)}{A(\mu \to \nu)} = 1 \tag{32}$$

, which is independent of the current and possible new state of the system and the temperature.

We can now chose $A(\nu \to \mu) = A(\mu \to \nu) = 1$, meaning that every move is always accepted. This is the reason why the Wolff algorithm performs better close to the phase transition than the Metropolis algorithm. The acceptance probability is always maximal, meaning the algorithm never wastes time to reject moves.

3.4 Monte Carlo simulation of Ising spins coupled to dynamical triangulations

In contrast to the Ising model on a regular lattice, a triangular lattice is dynamical and may react to temperature changes. Nevertheless, throughout the whole simulation the number of vertices and thus spins is kept constant, thus the system is still described by the canonical ensemble, and the Monte Carlo simulation techniques that have been discussed previously for the Ising model can be applied with slight adjustments.

Triangle moves

The move that allows the lattice to react to temperature changes is schematically depicted in figure (10).

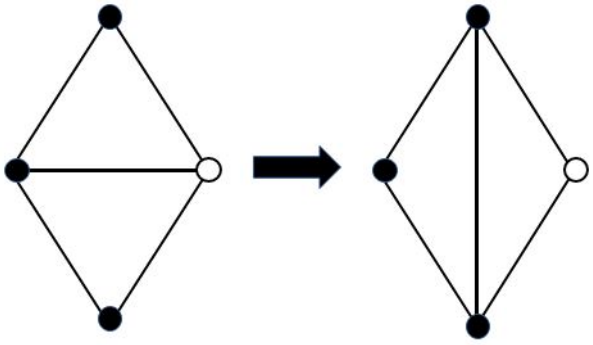

Figure 10: A random edge connecting an up (filled dot) and down (unfilled dot) spin is selected and flipped to connect two up spins according to a Metropolis-like acceptance probability.

The following list gives a recipe for this move:

1. Select a random edge k with probability g

$$g = \frac{1}{N} \tag{33}$$

, where N is the number of half edges. The selection probability is constant throughout the whole simulation and independent of the state λ the system is currently in.

2. Remove the edge with a probability $A(\lambda \to \sigma)$

$$A(\lambda \to \sigma) = \begin{cases} 1 & (\uparrow\downarrow) \text{ to } (\uparrow\uparrow),\ \Delta E \leq 0 \\ \exp\left(-\beta \Delta E\right) & (\uparrow\uparrow) \text{ to } (\uparrow\downarrow),\ \Delta E > 0 \end{cases} \tag{34}$$

and draw a new edge connecting the other two spins in the same phase to form the state σ.

A move lowering the total energy, $\Delta E < 0$, is always accepted, whereas a move that increases the energy, $\Delta E > 0$, is accepted with a probability that increases with temperature and decreases with increasing energy difference. Whether the energy change is positive, negative or zero, depends on the respective orientation of the spins on the vertices that are connected by the edge before and after the flip. Say the random edge selected is k and its adjacent half-edge is $\tilde{k}$, then the contribution to the total energy of the two half edges before the flip is E_λ

$$E_\lambda = S[k]\, S\left[\tilde{k}\right] \tag{35}$$

, where $S(k)$ denotes the spin value on the vertex from which the oriented half edge k is originating.

The energy after the flip is E_σ:

$$E_\sigma = S\left[n^{-1}(k)\right] S\left[n^{-1}(\tilde{k})\right] \tag{36}$$

Here, $n^{-1}(k)$ denotes the inverse of the next permutation n, which returns the previous edge in the clockwise direction of the same phase. Thus, the move is always accepted if the edge flipped connects two anti-aligned spins before the move and connects two aligned spins after the move (which lowers the total energy) or if the relative orientation of the spins is not altered, and the change in energy is equal to zero. The move is accepted with an exponential probability when the orientation changes from aligned to anti-aligned. Note again that each edge consists out of two oriented half edges; upon the move, both must be flipped clockwise.

3. Repeat

Wolff moves

To simulate the thermal fluctuation of the spins on a triangular lattice, the Wolff algorithm can be used as defined in section (3.1), but with slight adjustments. For the Ising model on a regular lattice, the spins considered to become members of the cluster were the four neighbours of the seed spin. On a triangular lattice, the number of neighbours depends on the degree of the vertex, which may vary throughout the simulation. All half-edges departing from a vertex, thus from the seed spin, must be explored. This can be done by acting the $n \circ a$ permutation on the seed-half-edge until one returns back to the same edge, thus until the permutation cycle is completed.

Combination of both moves

When implementing the algorithm, both the triangle flip move and the Wolff move needs to be combined. While doing so, one wants to distribute the computation time is equally between both parts of the simulation. At the beginning of each Monte Carlo move, we thus need to choose the triangle move with a probability P_{choose} or the Wolff move with a probability $1 - P_{\text{choose}}$, where P_{choose} is such that an equal distribution of computation time is ensured.

An edge flip is considered to require one time step, because at each move only one edge is adjusted. A Wolff move takes time in the order of the size of the cluster, because each spin needs to be flipped individually. Thus, on one Wolff move there should be ⟨clustersize⟩ edge flips performed, where ⟨clustersize⟩ denotes the average cluster size at a given temperature. The right probability to perform an edge flip is approximated by:

$$P_{\text{choose}} \approx \frac{\langle \text{clustersize} \rangle}{\langle \text{clustersize} \rangle + 1} \tag{37}$$

Note that this probability is dependent on the temperature, because the average cluster size take a maximal value at low and a minimal value at high temperatures.

3.5 Monte Carlo simulation of the Potts model coupled to dynamical triangulations

We can couple Potts spins to the vertices of a dynamical triangulation just as in the case of the Ising model. To study the thermal fluctuations of the resulting statistical system, the slight adjustments have to be made to the Monte Carlo techniques.

Spin moves

Just as the Ising model, the Potts model can be studied using the **Metropolis algorithm** [7], except that the selected spin is not multiplied by minus one, but a random value from the q possible ones is selected.

But also for the Potts model, the Metropolis algorithm slows down in the temperature region close to the phase transition. Additionally, due to the additional spin states, there is an other bottleneck introduced when q becomes large [7]. Suppose at some temperature T, there is a spin s_i selected on the lattice, of which all n nearest neighbours have a spin different from s_i and from each other. The algorithm should find the move that lowers the energy of the system, hence the spin s_i should flip to the same values of one of the neighbours.

The acceptance ratio for the Metropolis algorithm, however, is such that it accepts a final state with the same energy as the initial state with a hundred percent probability. As the new spin value during the flip move is chosen at random, it takes on average $\frac{q}{n}$ Monte Carlo steps to find a configuration that lowers the energy and stabilises the configuration, where n is the number of neighbours of the seed spin.

As for the Ising model, a **cluster algorithm**, like the Wolff algorithm, improves the performance in the critical region. The Wolff algorithm works again the same as for the Ising model, except with an adjusted probability P_{add}

$$P_{\text{add}} = 1 - e^{-\beta J} \tag{38}$$

to add the neighbour to the cluster. Here, a factor two has vanished in the exponential factor due to the re-scaling of the spin coupling constant J compared to the Ising model as shown in equation (6).

Triangle moves

For the triangle flip move, the way in which the energy is calculated needs to be adjusted to suit the Hamiltonian of the Potts model in equation (4). Whether the energy change is positive, negative or zero, still depends on the respective orientation of the spins on the vertices that are connected by the edge before and after the flip, but we do not have to calculate the product of the spin associated with a half-edge k and its adjacent $\tilde{k}$, but rather their Kronecker delta to obtain the energy for a state λ:

$$E_\lambda \propto \delta_{k,\tilde{k}} \tag{39}$$

The energy after the flip is E_σ

$$E_\sigma \propto -\delta_{n^{-1}(k),n^{-1}(\tilde{k})} \tag{40}$$

, where $n^{-1}(k)$ again denotes the inverse of the next permutation n. Therefore, the correct acceptance probability reads

$$A(\lambda \to \sigma) = \begin{cases} 1 & \Delta E = 0, -1 \\ \exp\left(-\beta \Delta E\right) & \Delta E = 1 \end{cases} \tag{41}$$

, where $\Delta E = E_\sigma - E_\lambda$.

3.6 Implementation and computational resources

This section contains background information on the coding process and the computational resources used. These experiences are personal, indicated by the use of the first person pronouns.

I started with implementing the Metropolis Algorithm (see section 3.2) for the Ising model on a regular lattice in C++ following the instructions of Newman and Barkema [7]. At that time, I was not familiar with the programming language C++, and thus acquired the necessary knowledge through 'learning by doing'. I tested the performance of the algorithm by measuring the magnetisation and its autocorrelation time and compared the results with those reported in [7].

In the second step, I implemented the Wolff algorithm (see section 3.3) for the two dimensional Ising model in C++ and tested the performance of the algorithm, again following Newman and Barkema's instructions.

Next, my supervisor Timothy Budd provided me with a C++ template, where dynamical triangulations and a triangle flip move are implemented. I then adjusted the code by coupling Ising spins to the vertices, adding the Wolff move on a triangular lattice and equipped the triangle flip move with the spin dependent acceptance probabilities (see section 3.4). I tested the performance by making first estimates of the magnetisation, Binders cumulant and other quantities.

Lastly, I generalised the above code to a q states Potts model coupled to a dynamical triangulation and performed detailed data analysis for $q = 2, 3, 4, 5, 10$. During this process, I often had to run long simulations. To do so, I was allowed to use the computing clusters of the high energy physics department. This included transferring files from my home computer to the computing cluster at the faculty and writing batch scripts.

4 Classification of Phase transitions

We have already briefly discussed the phase transition of the two dimensional Ising model in section (2.1). In the following section, means to classify and determine the order of phase transitions are introduced.

A phase transition takes place when macroscopic thermodynamic equilibrium quantities that function as an **order parameter** change qualitatively upon varying couplings of the system [12]. In the case of Ising and Potts models, the coupling is the temperature T [7] and the order parameter is the magnetisation.

4.1 Ehrenfest classification

Traditionally, phase transitions are classified by their order based on the **Ehrenfest classification** [12], named after the Austrian physicist Paul Ehrenfest (1880 - 1933) [13]. This classification makes use of the fact that macroscopic thermodynamic quantities can be described as partial derivatives of a suitable thermodynamic potential describing the systems response to changes in its environment.

According to Ehrenfest, an n-th order transition takes place when all $n-1$ partial derivatives of the potential with respect to a given intensive quantity of the system are continuous and if there is at least one of the n-th partial derivatives that is discontinuous for a given value of the coupling.

Practically, this classification succeeds in distinguishing first order from higher order transitions, but distinguishing higher order transitions from each other proves difficult in experiments [12]. Furthermore, transitions were found that could not be classified with the rules provided by Ehrenfest, as for example the logarithmic divergence in the two dimensional Ising model [12].

Thus, nowadays phase transitions are usually classified to be either continuous or discontinuous, where the former corresponds to a first order and the latter to a higher order Ehrenfest transition.

4.2 Determining the critical temperature T_c

It is not always as obvious from the graph of the order parameter as a function of temperature where the phase transition happens, as it is in the case of the 2D Ising model. For higher order continuous phase transitions, the graph can be smeared out, and there is no visible rapid drop down. Additionally, a limited accuracy of computer simulations effects the location of transition points.

To still get an estimate of the critical temperature, literature mentions two quantities that can be calculated from the average value of the order parameter: the binder cumulant $\mathscr{B}_A$ and U_4.

Binder cumulant $\mathscr{B}_A$

Let A be an order parameter of a statistical system, then $\langle A^k \rangle_L$ is a so-called **moment** of the order parameter probability distribution [14]. Here, k is some integer to the power of which the order parameter is raised before averaging, and L denotes the system size for which the order parameter has been measured. The moment associated with $k = 1$ may then e.g. be the magnetisation, and a combination of the $k = 1$ and $k = 2$ moments the magentic susceptibility.

Another quantity defined by the moments of the order parameter is the **binder cumulant** $\mathscr{B}_A$ defined [6] as

$$\mathscr{B}_A = \frac{1}{3}\left(1 - \frac{\langle A^4 \rangle}{\langle A^2 \rangle^2}\right) \tag{42}$$

, which is always negative or zero. The cumulant measures to which extent the probability distribution of the observable A deviates from a Gaussian shape [12].

The Binder cumulant is named after the physician Kurt Binder and is in earlier literature by Binder himself often referred to as the **fourth-order reduced cumulant** U_L [14], defined as:

$$U_L = 1 - \frac{\langle A^4 \rangle_L}{3\langle A^2 \rangle_L^2} \tag{43}$$

Literature also uses the renormalised coupling constant $g_L = -3U_L$, which has similar properties as U_L.

If the system size L tends towards infinity, the fourth-order reduced cumulant takes limiting values [14] as a function of temperature according to

$$\lim_{L\to\infty} U_L = \begin{cases} 0 & T > T_c \\ \frac{2}{3} & T < T_c \\ \in \left[0, \frac{2}{3}\right] & T = T_c \end{cases} \tag{44}$$

, where T_c denotes the critical temperature of the system.

Note that U_L differs from $\mathscr{B}_A$ by the positioning of the number three, thus the limiting cases of the Binder cumulat $\mathscr{B}_A$ are:

$$\lim_{L\to\infty} \mathscr{B}_A = \begin{cases} -\frac{2}{3} & T > T_c \\ 0 & T < T_c \\ \in \left[-\frac{2}{3}, 0\right] & T = T_c \end{cases} \tag{45}$$

For this thesis, we stick with the definition of $\mathscr{B}_A$ used by Jordan et. al [12].

When plotting the Binder cumulant as a function of temperature for various system sizes L, the curves intersect at one common point, which marks the critical temperature. This method is valid as well for continuous and discontinuous phase transitions [15]. The intersection point shifts with the system size as L^{-2d}, where d is the systems dimension. This shift is most often smaller then statistical errors. In the case that finite size effects do play a role, or the number of measurements is not high enough, a systematic scattering of intersection points [14] occurs, which means that the curves to not intersect in a well defined point and only a range for the critical temperature can be found.

Additionally, the cumulant may be used to qualitatively identify a discontinuous phase transition, as first shown by Vollmayr et. al. in 1993 [16]. If a certain critical system size L_{crit} is exceeded, the Binder cumulant of an order parameter of a statistical system showing a discontinuous phase transition develops a minimum. As L tends towards infinity this minimum shifts towards the critical temperature and becomes deeper and narrower.

Keutosis of the magnetisation U_4

A similar quantity to the binder cumulant is the Keutosis of the magnetisation U_4 defined [17] as

$$U_4 = \frac{\langle (M - \langle M \rangle)^4 \rangle}{\langle (M - \langle M \rangle)^2 \rangle^2} \tag{46}$$

, which takes its minimum value at the infinite volume value of the critical temperature. If the minimum value is bigger than one, it indicates a continuous phase transition.

Both quantities have been used to study the phase transition of the Potts model coupled to dynamical triangulations. By comparing the results for the classification of the phase transition to the expected orders from theoretical studies of the respective system, the validity of the criteria in a random geometry will be tested, while at the same time, data for the critical temperatures is obtained.

4.3 Using critical exponents to determine the order of a phase transition

Critical exponents [5] describe how thermodynamic quantities are scaling near the critical region. Theoretically, they can be calculated using a mean field approach or renormalisation group techniques. In practice, the exponents have to be determined using simulation data from finite systems. In this section, a technique to determine the exponent ν associated with the pseudocritical temperature and the correlation length and the exponent γ that governs the scaling of the magnetic susceptibility is discussed.

Critical exponent ν

The notion of a phase transition is only defined in the thermodynamic limit, thus for a system with an infinite volume. The critical temperature $T_c(\infty)$, that marks the temperature where the phase transition happens, is defined in this limit. A numerical simulation can only predict the **pseudocritical temperature** $T_c(V)$ for a finite system size V, which approaches $T_c(\infty)$ in the infinite volume limit.

To determine the exponent ν, the following scaling law [18] can be used:

$$T_c(V) - T_c(\infty) = -\left(\frac{1}{V}\right)^{\frac{1}{\nu}} \tag{47}$$

The critical exponent ν is approximately one for discontinuous transitions, as these transitions have a zero correlation length [12], whereas for continuous transitions the exponent ν deviates significantly from one [18]. In order to estimate the exponent ν, the system sizes simulated must resemble the behaviour of the system in the thermodynamic limit, hence must be chosen large enough. What constitutes a large enough system depends on how well the system under consideration resembles the infinite volume behaviour.

To apply the scaling law in (47), the pseudocritical temperature has to be determined for various system sizes. This can be done, for example, by measuring the temperatures for which the magnetic susceptibility is maximal. The magnetic susceptibility is the variance of the magnetisation and is defined as:

$$\chi = \frac{\beta}{N}\left(\langle M^2\rangle - \langle M\rangle^2\right) \tag{48}$$

When then plotting the difference between the pseudocritical temperature minus the infinite volume value of the critical temperature versus the inverse volume on a logarithmic scale, the critical exponent ν can be extracted from the slope of the linear graph. It is possible to fit for both ν and $T_c(\infty)$, but to do so more data points are needed than obtained within this thesis. The drawback of this is that the fit depends sensitively on the value of $T_c(\infty)$.

Critical exponent γ

To define the second exponent, we have to recall the properties of a continuous phase transition. Upon such a transition, the magnetic susceptibility diverges. The exponent γ measures how the maximum value of the magnetic susceptibility, defined in equation (48), scales with the size of the system.
The second exponent γ is defined [12] as

$$\chi \propto V^{\frac{\gamma}{\nu}} \tag{49}$$

, where χ is the maximum value of the magnetic susceptibility, V size of the system and ν the exponent that describes the scaling of the correlation length. For a discontinuous phase transition, the ratio $\frac{\gamma}{\nu}$ approaches one [17].

Inequalities

In fact, there are even more critical exponents that will not be considered here. Not all of them are independent of each other. The dependencies are expressed by inequalities, as e.g. the **Fisher inequality** [11] as given by

$$\gamma \leq (2-\eta)\nu \tag{50}$$

, which relates γ and ν to the critical exponent η, which, in specific cases, holds as an equality.

4.4 Universality of continuous phase transitions

When studying continuous phase transitions, we are interested in how thermodynamic quantities of the system behave (scale) near the phase transition [11]. For this, critical exponents are used. It seems that the value of these exponents depends on only a couple of parameters of the system and that they are independent of the microscopic details. This property is referred to as **universality**.

Universality [5] describes the phenomenon, that systems that may have different microscopic interactions still show the same qualitative behaviour near their continuous phase transition, and are thus described by the same set of critical exponents [11]. Systems with the same set of exponents, are said to be members of the same **universality class** [11].

There is not only one universality class, as the mean field approach suggested. Systems of different dimension, dimensionality of the order parameter, and range of microscopic interactions belong to different universality classes.

Universality was first demonstrated for the case of the two dimensional Ising model by L. Onsager [11]. Assuming an Ising model with an an-isotropic spin coupling constant J, thus it may be different in x and y direction, Onsager showed, that the critical exponent governing the divergence of the specific heat at the phase transition remained unchanged upon varying J_x and J_y, while only the amplitude was changing. With this he illustrated that the details of the microscopic interactions become less important at the critical point of the system.

Another example is the phase diagram of fluids, presented by E. A. Guggenheim [19]. The density of the coexisting phases plotted vs temperature does coincide for different fluids close to and far away from the critical point, when plotted in re-scaled units, see figure (11). Therefore, all eight fluids can be described with the same critical exponents.

Upon a continuous phase transition, the correlation length diverges. The correlation length describes the largest correlation in the system, thus if it is infinite, there are correlations on all length scales. These correlations dominate the system on every scale and the details of microscopic interactions become less relevant [11]. Because there are correlations on every length scale, the system is **scale invariant** when being exactly at the critical point [5]. In contrast, would the correlation length be finite, the range of interactions would change upon re-scaling the system. True scale invariance can therefore only occur if the correlation length is infinite or zero [5].

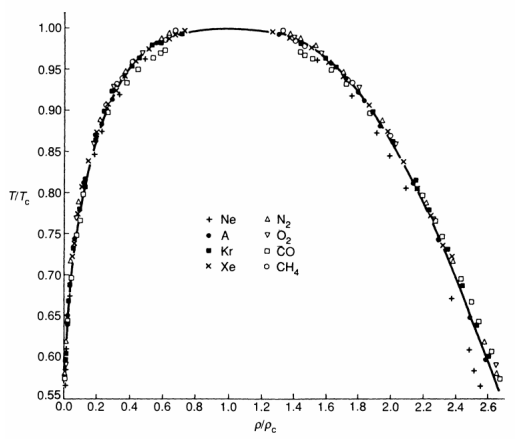

Figure 11: The density of coexisting phases plotted vs temperature in reduced units. the curves coincide for eight different fluids, indicating that the phase transitions belong to the same universality class. The data was obtained by Guggenheim [19], this picture was remade by Yeomans [5].

In practice, critical exponents [5] enable us to study the qualitative behaviour of a system with complex microscopic interactions, without modelling or even understanding them all in detail . Nevertheless, the exact value of the critical temperature T_c depends on the microscopic details [5]. A physical example for this is adsorbed mono-hydrogen on iron [5], which belongs to the same universality class as the two dimensional Ising model.

5 Formulation of the research question

The aim of this thesis can be divided into six sub-parts:

1. Illustrate the phase transition of the $q = 2,3,4,5$ and $q = 10$ states Potts models coupled to a dynamical triangulation using graphs obtained from a Monte Carlo simulation.

2. Determine the critical temperature of the Potts model coupled to dynamical triangulation for $q = 2,3,4,5$ and $q = 10$ using the Binder cummulant $\mathscr{B}_A$ and the Keutosis U_4 and compare the accuracy of the results, which is influenced by finite size effects.

3. Verify whether the Binder cumulant $\mathscr{B}_A$ develops a minimum for $q > 4$

4. Verify whether it can be shown that the Keutosis $U_4 > 1$ for the classification of a continuous phase transition holds by simulating the $q = 2,3,4,5$ and $q = 10$ states Potts model coupled to dynamical triangulations for up to $N = 32000$ triangles.

5. Measure the critical exponent ν for the $q = 2,3,4,5$ and $q = 10$ states Potts model coupled to dynamical triangulations using data for up to $N = 32000$ triangles, and verify whether the criterion that $\nu > 1$ for a continuous phase transition holds judging from this estimate.

6. Measure the ratio of critical exponents $\frac{\gamma}{\nu}$ for the $q = 2,3,4,5$ and $q = 10$ states Potts model coupled to dynamical triangulations using data for up to $N = 32000$ triangles.

6 Methods and the q=2 Potts model coupled to a dynamical triangulation

In this section the criteria to classify the order of phase transitions introduced in section (4) are applied to the $q = 2$ states Potts model coupled to a dynamical triangulation. This section functions as an introduction into the separate steps of the data analysis and sometimes reaches back to the Ising model on a square lattice for this purpose. Equipped with this example, in the next sections, the criteria will be applied to the Potts model coupled to dynamical triangulation for higher q to formulate answers to the aims of this thesis.

6.1 Preliminaries

Before the first measurements can be taken, the simulation has to be calibrated. This entails determining the equilibration time, measuring of the autocorrelation time and the estimation of the probability P_{choose}.

6.1.1 Equilibration

The goal of a Monte Carlo simulation is to sample states with the correct Boltzmann Probability. Thus, the simulation should be settled in its equilibrium, before taking measurements of thermodynamic quantities.

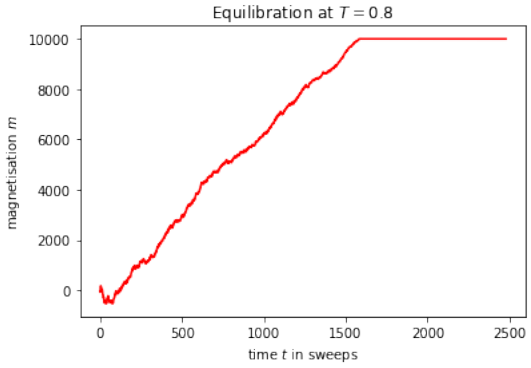

Figure 12: Equilibration of the magnetisaition of the two dimensional Ising model. Starting in a random spin configuration, it takes a certain equilibration time for the algorithm to settle into the energetically most favourable state.

Ising model on a square lattice

For the two dimensional Ising model this may look like as depicted in figure (12). A Metropolis algorithm simulation has been run for $T = 0.8$, where the system has started in a random spin configuration with magnetisation $M \approx 0$. Theory [7], predicts that for low temperatures, the energetically favourable state is where the majority of the spins are aligned. This causes the magnetisation to increase, until it has settled

in the energetically most favourable state, in which it remains for all future iterations. Therefore, it is essential to ensure that all measurements are taken after a long enough **equilibration time**.

Ising model on a dynamical triangulation

In a Monte Carlo simulation, the initial state of the system can be freely chosen. It is useful to start the simulation in a state that lies close to the equilibrium state of the system at that temperature to minimise the equilibration time.

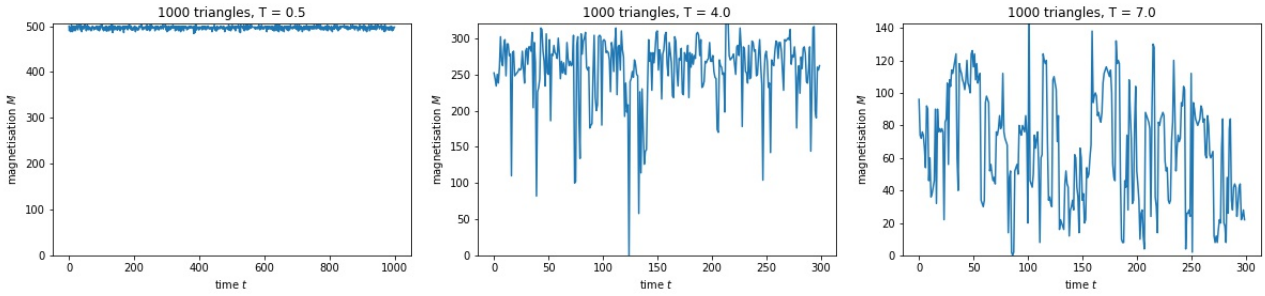

(a) *(b)* *(c)*

Figure 13: Equilibration of the magnetisation of the Ising model coupled to dynamical triangulation, measured for 1000 for the temperatures (a) $T = 0.5$, (b) $T = 4.0$, (c) $T = 7.0$

For the Ising model coupled to a dynamical triangulation, the simulation has been run for increasing temperatures. Initially, all spins are aligned, which is the system's state at low temperature and no equilibration time is need. Then, when completing the first temperature run, the spin state is stored and passed as an initial state to the next run with a higher temperature. By doing so, the system always starts in a state that is already close to the equilibrium state. When measuring the equilibration time for the Ising model coupled to a dynamical triangulation, no equilibration time can be detected, as shown in figure (13). This procedure is also applied to all measurements for the Potts model.

To avoid measuring in a non equilibrium state, 500 sweeps (1 sweep = N Monte Carlo steps) are performed for each temperature before starting to measure.

6.1.2 Autocorrelation

The time it takes until two configurations are truly independent of each other can be determined with the **autocorrelation function** [7] $\chi(t)$.

$$\chi(t) = \int d\tilde{t}\left[m(\tilde{t})m(t+\tilde{t}) - \langle m\rangle^2\right] \tag{51}$$

The autocorrelation function is an equilibrium quantity [7], thus only those measurements of the magnetisation, which have been obtained after long enough equilibration time may be used to calculate it.

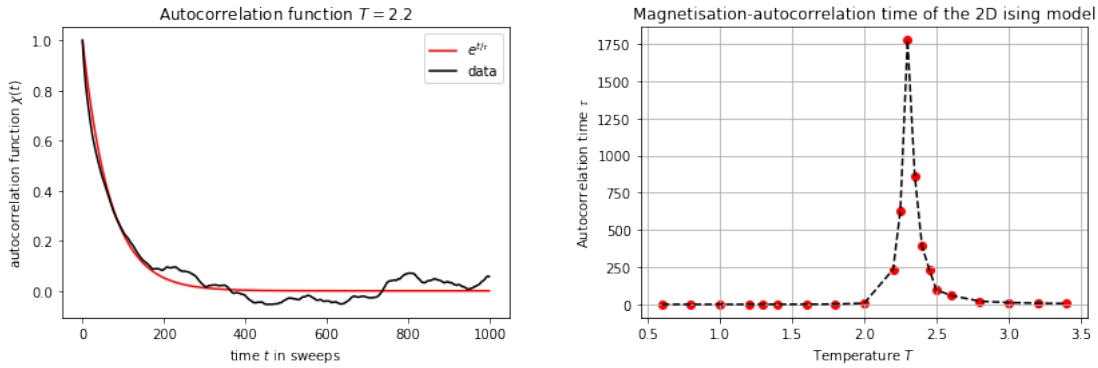

(a) *(b)*

Figure 14: Autocorrelation function of the magnetisation at $T = 2.2$ (a) and autocorrelation time vs temperature (b) of the 10 times 10 two dimensional Ising model measured with the Metropolis Algorithm.

Two dimensional Ising model on a square lattice

Figure (14a) shows the autocorrelation function of the magnetisation for the two dimensional Ising model at $T = 2.2$ as simulated with the Wolff algorithm. The function has been normalised by its value $\chi(0)$ at $t = 0$ to start at the value one. It can be seen that, over time, the correlation function drops exponentially. To estimate a typical time scale, the **correlation time** τ, a fit with the exponential function

$$\chi(t) = \exp\left(\frac{t}{\tau}\right) \tag{52}$$

can be done. The autocorrelation time τ then measures, how long it takes until the correlation between two states has dropped by $\frac{1}{e}$ of the initial value $\chi(0)$.

Then, two states are considered to be independent [7] if they are at least two autocorrelation times separated from each other.

Note that averaging over values that are correlated is nothing wrong. However, adding correlated measurements does not improve the estimate of a time averaged quantity, here the magnetisation. By taking measurements only after each 2τ, the simulation can be sped up significantly by saving measurement time.

Figure (14b) shows the autocorrelation time τ of the two dimensional Ising model on a square lattice as a function of temperature determined using a fit to equation (52). Recall that the phase transition happened at a critical temperature of about $T_c \approx 2.3$, which is exactly where the autocorrelation time increases rapidly. Further away from the phase transition, the correlation time is almost zero.

Near the phase transition, the Metropolis algorithm is slowing down [7], as shown in section (2.2): the correlation time increases, because the statistical fluctuations of the Ising model itself are maximal in the critical region, which implies that more measurements are needed for an accurate estimate of the order parameter, then there would be necessary further away from the critical region.

$q = 2$ *states Potts model coupled to a dynamical triangulation*

A similar behaviour can be observed for the $q = 2$ states Potts model coupled to a dynamical triangulation. The autocorrelation function is calculated from 300 measurements of the magnetisation that are taken in time steps of ten sweeps. This is repeated three times for each of the system sizes, $N = 1000, 2000, 4000$ and $N = 8000$ triangles, and the autocorrelation times at each temperature are averaged.

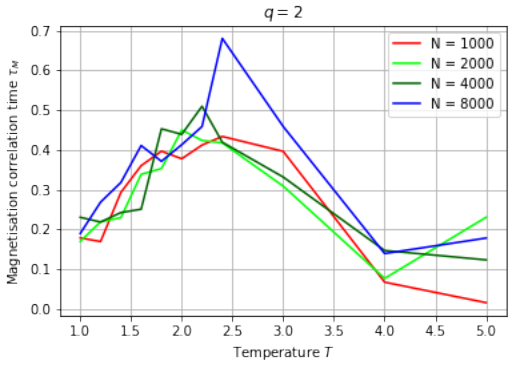

Figure 15: Magnetisation autocorrelation time in time steps of 10 *sweeps versus temperature for the* $q = 2$ *states Potts model coupled to a dynamical triangulation measured for four different number of triangles* N.

The result is shown in figure (15). The peak in the magnetisation autocorrelation time is not as sharp as for the two dimensional Ising model on a square lattice, but a significant increase can be seen. It can be seen that the autocorrelation time tends to increase for an increasing system size. This is a feature of the finite size of the simulation, which estimates with increasing N the theoretical infinite volume properties of the system with increasing accuracy. Based on these estimates for the autocorrelation time, it was chosen to perform measurements of the magnetisation every 30 sweeps.

For the simulations, it is only necessary to obtain a rough estimate of the autocorrelation time, as the time between two measurements may be chosen larger than the autocorrelation time to be on the safe side. For all measurements of the Potts model on a triangulation the time between measurements is taken to be between 30 and 40 sweeps.

6.1.3 Probability to perform a triangle flip move P_{choose}

To distribute the computation time equally between triangle flip and Wolff moves, the probability P_{choose}. A way to determine the value of this probability is measuring it during the equilibration phase of the simulation using (37), and store the value.

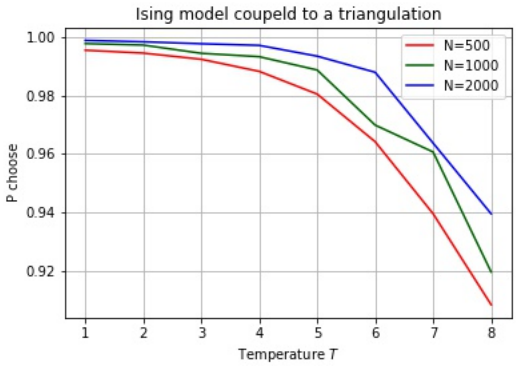

Figure 16: The probability to perform a triangle flip move P_{choose} as a function of temperature, measured for the Ising model coupled to a dynamical triangulation.

Figure (16) shows the Probability P_{choose} of the Ising model coupled to dynamical triangulations as a function of temperature. Recall that the probability depends on the average cluster size in the Wolff algorithm. With increasing temperature, the spins on the triangulation become randomly oriented with respect to each other. The number of neighbours of a given seed spin that are added with an acceptance probability of one to the cluster decreases. Therefore, also the size of the cluster tends to decrease, and so does the

probability P_{choose}. The plot shows that the probability is also affected by finite size effects, as the cluster size of larger systems tends to decrease slower.

During a Wolff move, a random half-edge has to be selected, and then all half-edges departing from the same vertex have to be determined and considered as members of the cluster. For a triangle flip, a half-edge is selected and flipped, if the move has been accepted. Therefore, even for the smallest cluster of size one, a Wolff moves takes longer then a triangle flip. In the rare case, where the vertex degree is equal to one, both moves take a similar amount of time. Considering this, the behaviour of the probability P_{choose} implies a slowing down of the algorithm with increasing temperature, as there have to be more Wolff moves performed to distribute the computation time equally.

For the measurements for the other q values, P_{choose} is evaluated during the equilibration phase of each temperature, stored and applied to the simulation afterwards.

6.1.4 Error analysis with the Bootstrap method

Before starting with the data analysis, a way to estimate the statistical error on the measurements is required. Therefore, this section introduces the **Bootstrap** method [7] for error estimation in a Monte Carlo simulation.

All quantities that need to be measured for this project are thermodynamic equilibrium quantities that are defined by their expectation value in the thermodynamic limit. To obtain an infinitely accurate measurement for an expectation value, an infinite amount of measurement at an infinite system size is required, which is impossible. Still, the error in the averaged quantities should decrease with an increasing number of measurements and system size.

To calculate the statistical uncertainty resulting from a finite amount of measurements, there is usually one of two methods used: the Jackknife or Bootstrap method [7]. In this project, the Bootstrap method is applied, as it is seen as the most efficient method [7] and it is also applicable if the measurements are correlated.

The goal is to estimate the error of a quantity B derived from a time sequence of n measurements of a parameter say A. Think for example of the magnetisation M which is measured at n time steps during the Monte Carlo simulation. The quantity of interest could then be the average magnetisation $\langle M \rangle$.

One picks out n measurements at random from the time sequence of A, while duplicates are allowed. Then the quantity B, is calculated using this **resampled** data. This is repeated x times. Then one obtains x slightly different values of the quantity B.

The error in B is then estimated by the standard deviation σ of the x values, defined as

$$\sigma = \sqrt{\langle B^2 \rangle - \langle B \rangle^2} \tag{53}$$

, where the angle brackets indicate the average over the x values of B or B^2 respectively.

Note that the standard deviation described by equation (53) does not depend on the number of re-samplings, as it would be wrong to suppose that the statistical error decreases just by performing more re-samplings [7], hence by increasing x. Instead, the error σ should approach a fixed value as a function of the re-samplings x. This is also how one can judge whether enough re-samplings have been performed. Additionally, one can average over the x values of B to obtain a more accurate estimate.

The Bootstrap method can only be used to estimate statistical errors in the system. Sometimes, the systematical error is larger then the statistical one, e.g. due to finite size effects, and will be considered during the analysis, if necessary.

6.2 Magnetisation and magnetic susceptibility

Being equipped with an estimate of the equilibration and autocorrelation time and a way to determine the probability P_{choose} for each temperature, measurements of the magnetisation can be made.

Magnetisation

Figure (17) shows the magnetisation of the $q = 2$ states Potts model as a function of temperature for $N = 1000, 2000, 4000, 8000, 16000$ and $N = 320000$. Ten thousand measurements are taken every 30 sweeps for a range of temperatures between $T = 1.0$ and $T = 6.0$.

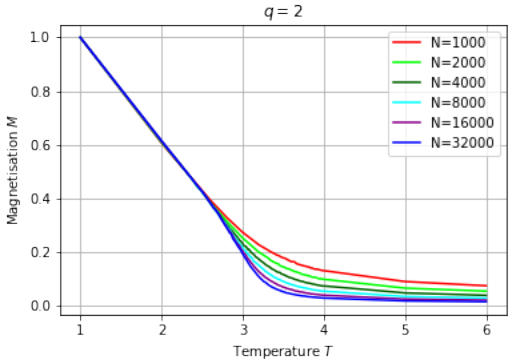

Figure 17: Magnetisation as a function of temperature of the $q = 2$ states Potts model for six different system sizes between $N = 1000$ and $N = 32000$.

The magnetisation has been normalised by its value at $T = 1$ causing the curves to start at a magnetisation of $M = 1$. Compared to the magnetisation of the two dimensional Ising model on a square lattice, there is no step function behaviour. The magnetisation is still an order parameter of the system, but the phase transition is not clearly visible as the curve is smeared out. However, the magnetisation approaches zero for increasing temperatures.

The critical temperature and the order of the phase transition can not be read off directly from the curve of the magnetisation. To determine them, the criteria introduced in section (4) will be applied to determine the critical temperature in the next section.

Note that the magnetisation is dropping to zero faster with increasing system size. This is a feature of the finite size of the lattice. With an increasing number of triangles, the infinite volume properties are approximated more accurately.

Magnetic susceptibility

The magnetic susceptibility measures the standard deviation of the magnetisation as a function of temperature. It can be calculated straightforwardly from the measurements of the magnetisation using formula (48).

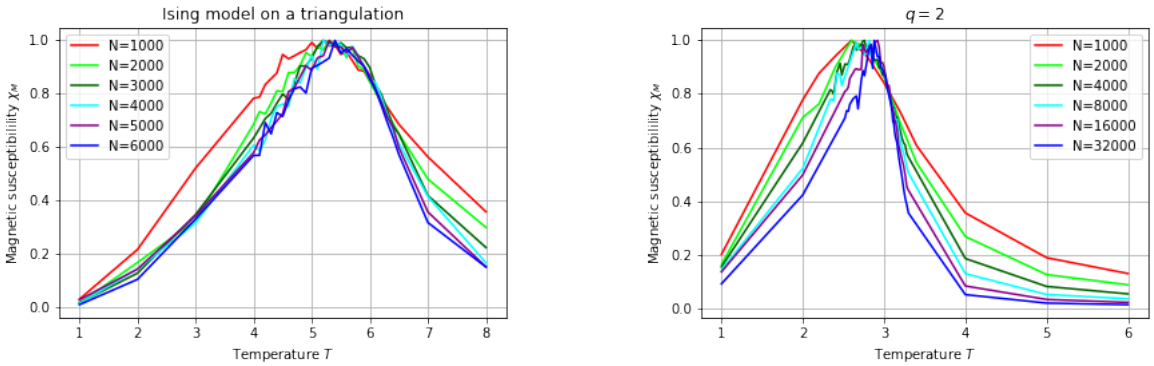

Figure 18: Normalised magnetic susceptibility of the Ising (a) and $q = 2$ states Potts model (b) coupled to dynamical triangulations.

Figure (18) shows the magnetic susceptibility as a function of temperature for the Ising model and the $q = 2$ states Potts model, both coupled to dynamical triangulations.

First of all, there is actually no qualitative difference between the two different models, as we have seen in section (2.2), as only the spin coupling constant J has been re-scaled and a constant quantity has been added to the Hamiltonian. Therefore, only the $q = 2$ states Potts model will be considered in the further analysis.

For each system size, the susceptibility has been normalised by its maximum value to compare the shape of the curves for increasing N. The peak becomes narrower with increasing N, and that the maximum shifts to the right. This is again a finite size effect. Theoretically, for an infinitely big system, the magnetic susceptibility would diverge at the critical temperature. Note that in the plots it seems that the magnetic susceptibility is fluctuating more rapidly near its maximum. This is not the case, as this results from the fact that the temperature steps with which the magnetisation has been measured is chosen smaller near the maximum, to determine its position more accurately.

The position of the peak marks the quasi critical transition point of the finite sized system, and plays a significant role in determining the critical exponent ν introduced in section (4).

6.3 Binders cumulant $\mathscr{B}_A$

From the magnetisation measurements, the Binder cumulant has been be calculated. Figure (19) shows

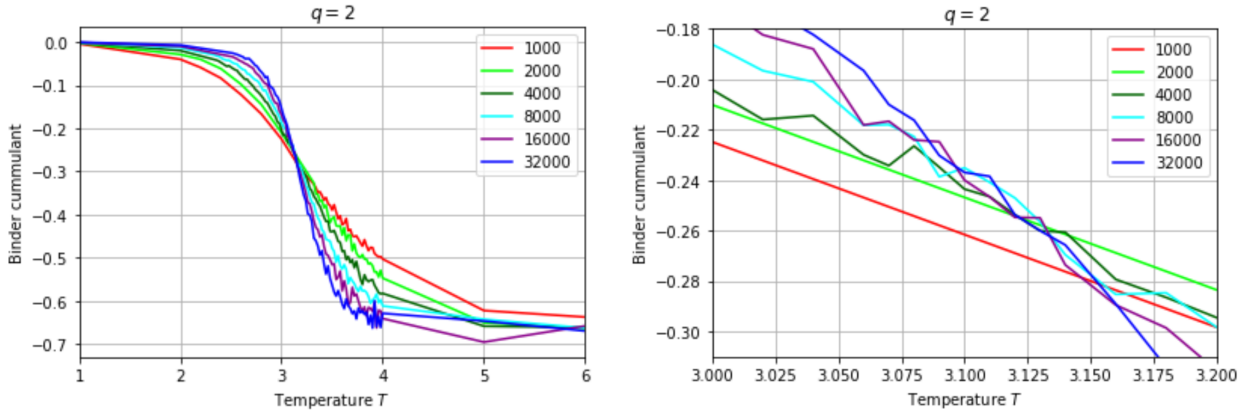

Figure 19: Binder cumulant of the q = 2 states Potts model coupled to a dynamical triangulation (a) and (b) zoomed in onto the intersection point.

the Binder cumulant for the $q = 2$ states Potts model coupled to a triangulation. Note, that the Binder cumulant seems to fluctuate. This is again due a narrow spacing of the measurement points. The cumulant indeed obeys the limit criteria formulated in equation (45).

As a systematic scattering of the intersection point occurs, only a range for the critical temperature is determined by zooming in on the graph, see figure (19b). The critical temperature range is read by eye to be between $T = 3.075$ and $T = 3.105$ for $q = 2$.

Additionally the binder cumulant for $q = 2$ does not develop a clear minimum for the system sizes and temperatures considered.

6.4 The Keutosis U_4

This section introduces on the analysis of the Keutosis U_4 of the magnetisation.

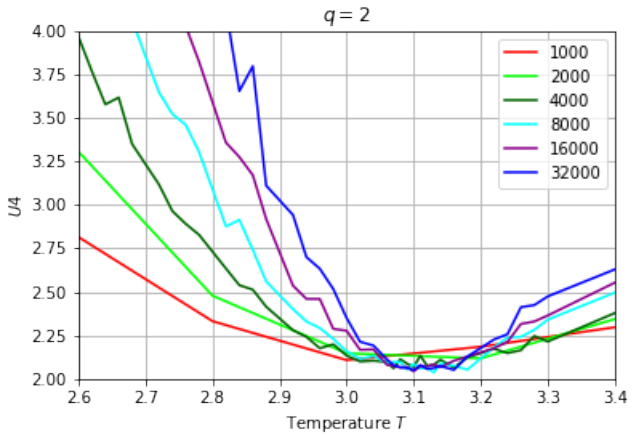

Figure 20: The Keutosis U_4 of the magnetisation as a function of temperature for the $q = 2$ states Potts model.

Figure (20) shows U_4 of the magnetisation for the $q = 2$ states Potts model. A minimum is visible, which is affected by finite size effects. The minimum becomes more narrow and shifts to the right with increasing system size.

The Keutosis U_4 has a minimum located at the critical temperature. Additionally, the minimum value gives an indication of the order of the phase transition. Therefore, the goal is to determine the minimum value of U_4 as well as the temperature at which it occurs. To determine both quantities, two different methods, a polynomial fit and a spline interpolation, are applied.

Polynomial fit

For the first method, a polynomial with a suitable degree was fitted to the region of U_4 where the minimum is situated. The minimum is then determined by evaluating where the derivative is equal to zero.
For the $q = 2$ states Potts model, the suitable polynomial degrees are $= [2,2,2,2,2,4]$, ordered for increasing N. The degree of the suitable polynomial tends to be higher for increasing N, because then the minimum is sharper defined.

Spline interpolation

The second method interpolates the measured point with a univariant spine of degree 2, as implemented by the scipy package in python. The implementation comes with the change to set a 'smoothing factor', which determines how much the spline is smoothing to the data points. For $q = 2$ the suitable smoothing factors are $[0.003, 0.05, 0.1, 0.1, 0.1, 0.5]$.

Observations on the critical temperature

The resulting values for the critical temperature and the minimum values of U_4 for both methods are summarised in table (1).

Table 1: Fit values for the minimum of U_4 for the $q = 2$ state Potts model coupled to a dynamical triangulation. For the fit the degrees $[2,2,2,2,2,4]$ and for the interpolation the smoothing factors $[0.003, 0.05, 0.1, 0.1, 0.1, 0.5]$ have been used. The errors are estimated with the Bootstrap method, and 70 resamplings have been done.

N	fit	interpolation	fit	interpolation
1000	$T_c = 3.048 \pm 0.006$	$T_c = 3.06 \pm 0.03$	$\min(U_4) = 1.92 \pm 0.02$	$\min(U_4) = 2.12 \pm 0.02$
2000	$T_c = 3.09 \pm 0.01$	$T_c = 3.14 \pm 0.03$	$\min(U_4) = 1.91 \pm 0.03$	$\min(U_4) = 2.09 \pm 0.02$
4000	$T_c = 3.051 \pm 0.008$	$T_c = 3.10 \pm 0.015$	$\min(U_4) = 1.97 \pm 0.02$	$\min(U_4) = 2.093 \pm 0.008$
8000	$T_c = 3.047 \pm 0.008$	$T_c = 3.11 \pm 0.02$	$\min(U_4) = 1.90 \pm 0.03$	$\min(U_4) = 2.061 \pm 0.008$
16000	$T_c = 3.078 \pm 0.007$	$T_c = 3.10 \pm 0.05$	$\min(U_4) = 1.89 \pm 0.03$	$\min(U_4) = 2.0 \pm 0.1$
32000	$T_c = 3.130 \pm 0.003$	$T_c = 3.10 \pm 0.01$	$\min(U_4) = 2.02 \pm 0.02$	$\min(U_4) = 2.07 \pm 0.03$

It can be observed that the location of the minimum of U_4 is indeed affected by finite size effects, while the deviations decrease with increasing system size.

Observations on the minimum value of U_4

As for the order of the phase transition, the minimum value of U_4 is greater than one, which indicates a continuous phase transition. According to [2] the phase transition of the $q = 2$ state Potts model coupled to a triangulation is expected to be a continuous one. Thus the U_4 criteria predicts the right order in this scenario.

6.5 Critical exponents

In this section the methods to determine the critical exponents ν and $\frac{\gamma}{\nu}$ are introduced and the results for the $q = 2$ states Potts model are shown.

To perform the power law fits, first the quasi critical temperature and the maximal value of the magnetic susceptibility need to be determined. They can be found by determining the location and height of the maximum of the magnetic susceptibility as a function of the volume. To do so, the fit and spline interpolation method is applied, as already has been used to fit the minimum of U_4.

Estimation of the critical exponent ν

The results for the critical temperature, measured by determining the location of the maximum of the magnetic susceptibility with a polynomial fit and a spline interpolation are shown in figure (21). It can be seen that the pseudocritical temperature approaches a maximal value, which would be the critical temperature in the infinite volume limit. The errors are determined from 70 resamplings of the bootstrap method.

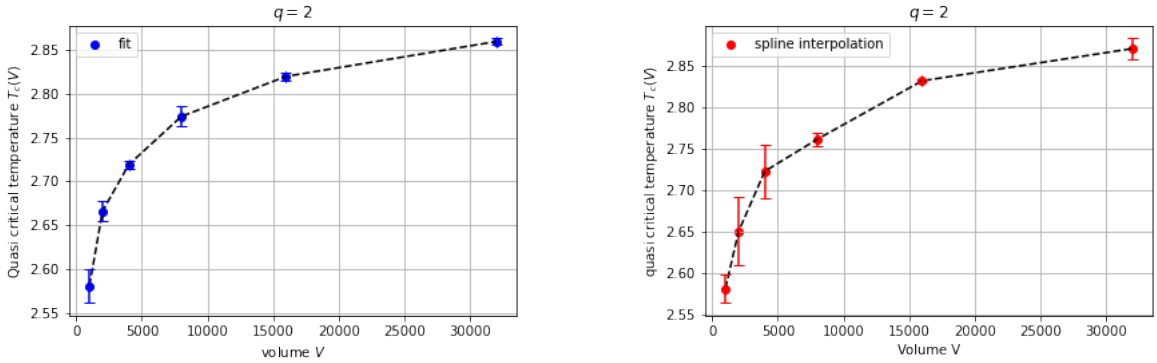

Figure 21: The location of the maximum of the magnetic susceptibility of the $q = 2$ states Potts model is determined with a polynomial fit of degree $[8,8,8,10,8,8]$ *and a spline interpolation with smoothing factors* $[5\cdot10^4, 5\cdot10^4, 1\cdot10^7, 6\cdot10^8, 6\cdot10^9, 4\cdot10^{10}]$.

The interpolation method returns larger errors for the lower temperatures, this is partially due to an increased spacing of the temperature for $N = 1000$ and $N = 2000$, as the data is affected by finite size effects, and the spline interpolation tends to perform better, if more data points are present. Nevertheless, the interpolation method is included for all analysis to have a second estimate, and to make sure that the fit method does not entail any systematical errors (overfit, etc).

When plotting the logarithm of the quasi critical temperature versus the logarithm of 1/V, the critical ex-

ponent ν can be extracted from the slope of the resulting line.

To perform the fit, however, the infinite volume critical temperature is required, compare equation (47). From the Binder cumulant and U_4 analysed in the previous section, the critical temperature cannot be determined definitely, and the two methods do not always agree with each other within the statistical error margin. This indicates that the systematical error is significant for the determination of the critical temperature, which is introduced by finite size effects. To account for this error, a range for the critical temperature is determined for both methods. For the Binder cumulant the procedure has already been described in section (6.3). For U_4, the fit and interpolation values of the two biggest system sizes $N = 16000$ and $N = 32000$ with a at least one digit precision are considered. The ranges for the critical temperatures are shown in table (2).

Table 2: Minimal and maximal values for the critical temperature for the $q = 2$ states Potts model as determined by the Binder cumulant and U_4.

	$\min(T_c)$	$\max(T_c)$
Binder	3.075	3.105
U_4	3.100	3.130

The linear fit to estimate the exponent ν is done for the values of T_c determined ranges in steps of 0.001. Next, the systematical error is estimated as

$$\sigma = \frac{\max(\nu) - \min(\nu)}{2} \tag{54}$$

which measures the width of the range of ν that results from the uncertainty in the critical temperature.

The statistical error is estimated by performing 70 re-samplings using the bootstrap method for the determination of the quasi critical temperature. The fit for ν is done for each of the 70 set of data points.

The resulting values for ν are than averaged, and this is the value given in table (3). The error indicated in the table is either statistical or the systematical error, depending on which one of the two is larger.

Table 3: The critical exponent ν for the $q = 2$ states Potts model measured with a fit and interpolation method.

	Binder	U_4
fit	4.4 ± 0.2 (sy = st)	4.8 ± 0.2 (st)
interpolation	4.1 ± 0.3 (sy)	4.4 ± 0.3 (sy)

Estimation of the critical exponent $\frac{\gamma}{\nu}$

To measure the ratio $\frac{\gamma}{\nu}$, the maximum of the magnetic susceptibility needs to be extracted from the data and plotted against V. Then, a fit can be performed to match the power law in equation (49). The exponent γ can then be estimated using the fitted value for ν of the previous analysis.

From the same fit and interpolation method as used to determine the quasi critical temperature in the previous part, the maximum of the magnetic susceptibility is measured as a function of the volume.

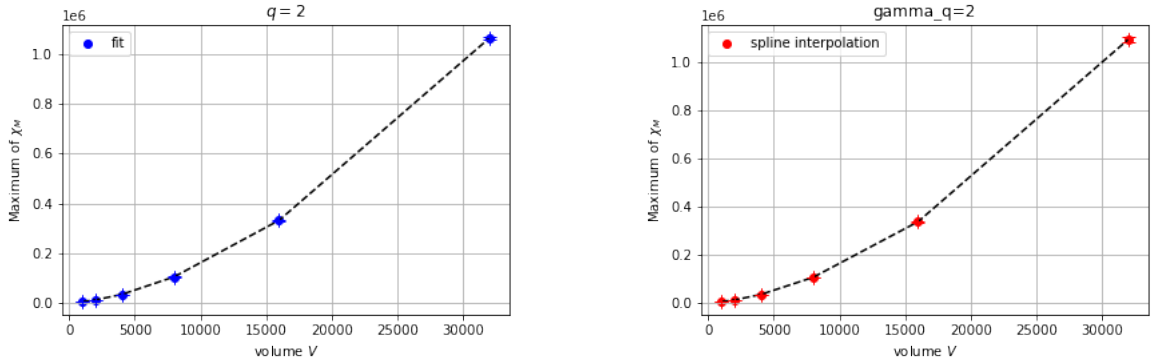

Figure 22: The maximum of the magnetic susceptibility of the $q = 2$ states Potts model is determined with a polynomial fit of degree $[8,8,8,10,8,8]$ *and a spline interpolation with smoothing factors* $[5\cdot10^4, 5\cdot10^4, 1\cdot10^7, 6\cdot10^8, 6\cdot10^9, 4\cdot10^{10}]$.

The results for both methods are shown in plots in figure (22). The maximum of the magnetic susceptibility increases as a function of the volume. In the infinite volume limit, the magnetic susceptibility diverges [11], thus the maximum approaches infinity.

The ratio of critical exponents $\frac{\gamma}{\nu}$ is determined for both methods by a power law fit to these curves give rise to the values summarised in table (4) where the error is in both cases the statistical error determined by 70 re-samplings of the bootstrap method.

Table 4: The ratio of the critical exponents $\frac{\gamma}{\nu}$ for the $q = 2$ states Potts model on a dynamical triangulation, determined using a fit and interpolation method.

q	fit	interpolation
2	$\frac{\gamma}{\nu} = 1.675 \pm 0.003$	$\frac{\gamma}{\nu} = 1.701 \pm 0.005$

7 Results for the q states Potts model coupled to a dynamical triangulation

This section shows the results of the same analysis as in the previous section but then for the $q = 3, 4, 5$ 10 states Potts model. The analysis is summarised and for detailed plots and fitting values as well as the equilibration and autocorrelation, analysis the reader is referenced to the appendix. For completeness and to enable an easy comparison between the different q values, the results for $q = 2$ found in the previous sections are repeated in the tables.

7.1 Binders cumulant $\mathscr{B}_A$

The minimal and maximal values for the intersections for all measured q values are summarised in table 5.

Table 5: Minimal and maximal value for the intersection determined with the Binder cummulant.

q	$\min(T_c)$	$\max(T_c)$
2	3.075	3.105
3	2.743	2.744
4	2.520	2.525
5	2.374	2.380
10	2.010	2.035

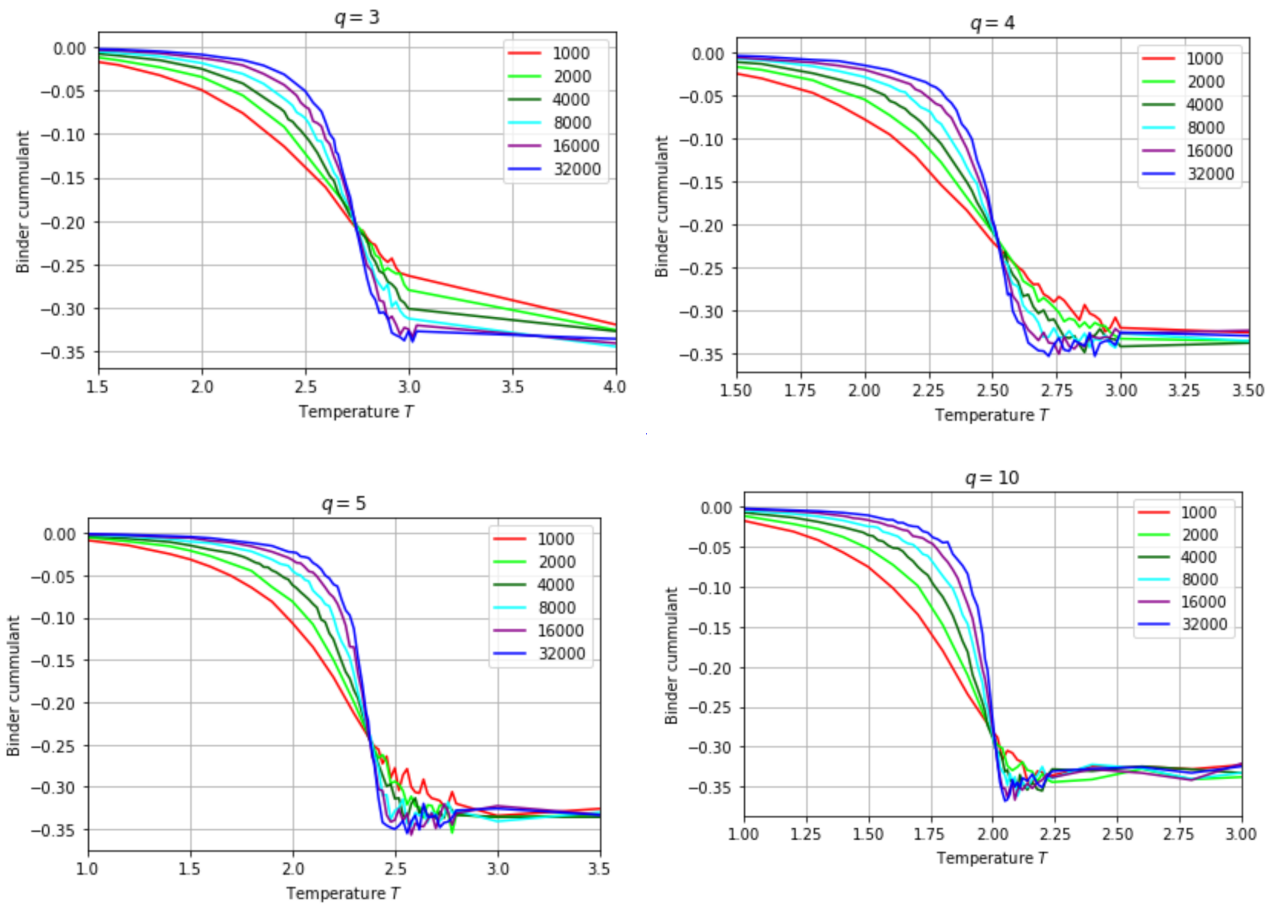

Figure 23: Binder cummulant of the magnetisation for $q = 3,4,5,10$ *measured for system sizes ranging between* $N = 1000$ *and* $N = 32000$.

Figure (23) shows the graphs for the binder cumulant of the magnetisation for $q = 3,4,5,10$. The graphs of the binder cummulant for $q = 5,10$ seem to show a minimum for the measured system sizes, which appears after exceeding a critical system size. The minima become deeper and narrower slowly. For $q = 3$, there is no clear minimum visible. For $q = 4$, the case is inconclusive, because measurements are missing for $T > 3$.

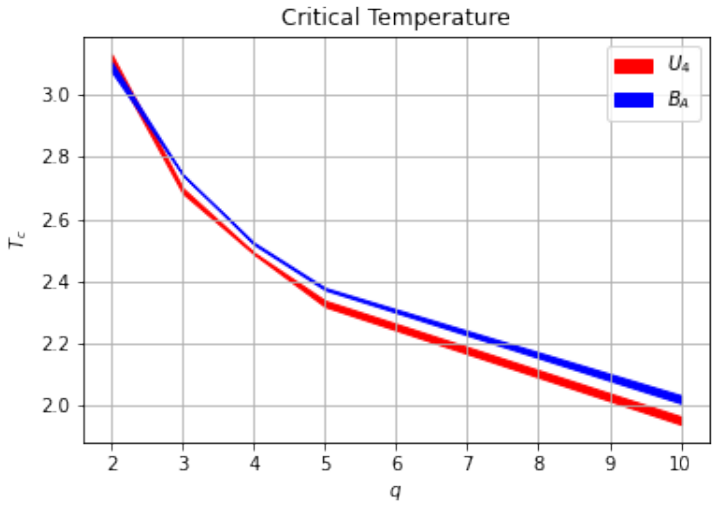

Figure 24: The critical temperature as a function of the number of states q as determined with the Binder cumulant and the Keutosis. The thickness of the curve indicates the uncertainty in the critical temperature.

7.2 The Keutosis U_4

Interesting for the fit of ν are the minimal and maximal values of T_c that have been determined for various q from the minim of U_4 with the two different fit methods. The results are summarised in table (6). The detailed results and graphs of the fit and interpolation are listed in appendix (A.7).

Table (7) summarises the absolute minimal value of U_4 found for each q with at least a one digit precision, where the smallest error is denoted in the cases that the value occurred multiple times.

Additionally, figure (24) summarises the minimal and maximal value for the critical temperature as a function of the number of states q for the Keutosis and the Binder cumulant. Note that the Potts model is only defined for integer values of q, the graph is drawn also at non integer values to guide the eye.

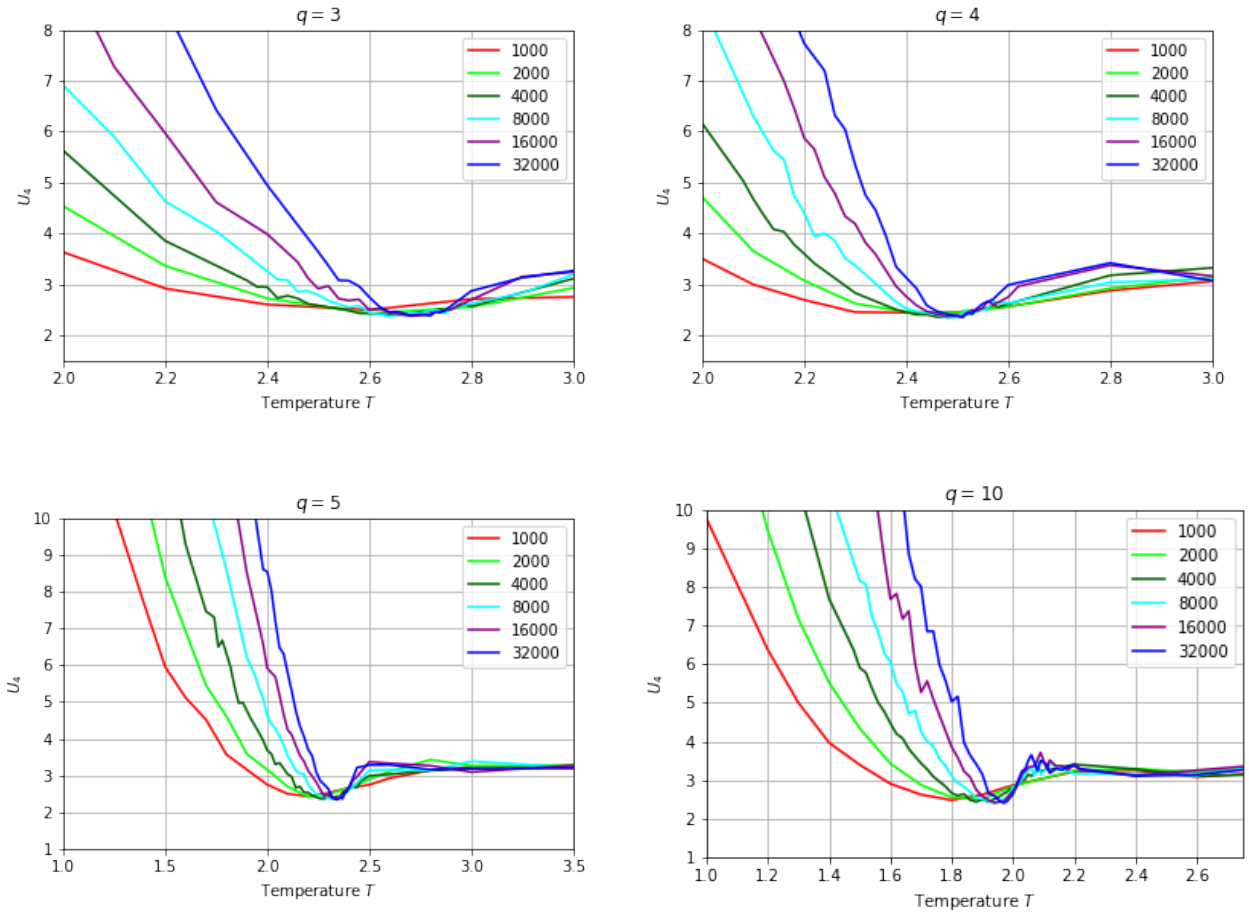

Figure 25: The Keutosis U_4 of the magnetisation for $q = 3, 4, 5, 5$ for $N = 1000, 2000, 4000, 8000, 16000, 32000$ triangles.

Table 6: Minimal and maximal value for the intersection determined with U4.

q	$\min(T_c)$	$\max(T_c)$
2	3.100	3.130
3	2.684	2.700
4	2.489	2.493
5	2.320	2.339
10	1.942	1.967

Table 7: The absolute minimal value of U_4 for the $q = 2,3,4,5,10$ states Potts model coupled to a dynamical triangulation.

q	$\min(U_4)$
3	2.07 ± 0.03
3	2.38 ± 0.01
4	2.37 ± 0.02
5	2.36 ± 0.03
10	2.3 ± 0.3

7.3 Critical exponents

Determining ν

The results for the critical exponent ν of the $q = 3,4,5,10$ states Potts model coupled to a triangulation for the fit and interpolation method are summarised in table (8). Detailed plots are shown in appendix (A.5).

Table 8: The critical exponent ν for $q = 3,4,5,10$. After each value the type of the error is indicated in brackets. A systematical error is denoted as '(sy)', a statistical error as '(st)'.

	Method	**Binder**	**U4**
q=2	fit	4.4 ± 0.2 (sy = st)	$\nu = 4.8 \pm 0.2$ (st)
	interpolation	4.1 ± 0.3 (sy)	$\nu = 4.4 \pm 0.3$ (sy)
q=3	fit	3.64 ± 0.08 (st)	$\nu = 3.0 \pm 0.1$ (sy)
	interpolation	3.9 ± 0.4 (st)	$\nu = 3.2 \pm 0.1$ (sy)
q=4	fit	4.5 ± 0.1 (st)	$\nu = 4.1 \pm 0.1$ (st)
	interpolation	3.9 ± 0.3 (st)	$\nu = 3.5 \pm 0.4$ (st)
q=5	fit	3.56 ± 0.9 (st)	$\nu = 3.0 \pm 0.1$ (sy)
	interpolation	3.6 ± 0.2 (st)	$\nu = 3.0 \pm 0.2$ (sy)
q=10	fit	4.9 ± 0.2 (st)	$\nu = 4.0 \pm 0.2$ (sy)
	interpolation	7 ± 1 (st)	$\nu = 5.7 \pm 0.7$ (st)

For $q = 4$, the interpolation estimate based on U_4, has been determined without the data point at $N = 32000$, as the interpolation method has caused significant errors for the maximum of the magnetic susceptibility.

For $q = 10$, the interpolation method performed badly to determine the maximum of the magnetic susceptibility. The errors are large (see appendix (A.5)) and thus the value for ν is unreliable.

Determining $\frac{\gamma}{\nu}$

The results for the ratio of critical exponents $\frac{\gamma}{\nu}$ are summarised in table (9). For all values, the error is determined by performing 70 re-samplings with the Bootstrap method. Detailed plots can be found in appendix (A.6).

Table 9: Results of the ratio of $\frac{\gamma}{\nu}$ *for* $q = 3, 4, 5, 10$.

q	**fit**	**interpolation**
2	$\frac{\gamma}{\nu} = 1.675 \pm 0.003$	$\frac{\gamma}{\nu} = 1.701 \pm 0.005$
3	$\frac{\gamma}{\nu} = 1.622 \pm 0.008$	$\frac{\gamma}{\nu} = 1.61 \pm 0.01$
4	$\frac{\gamma}{\nu} = 1.58 \pm 0.01$	$\frac{\gamma}{\nu} = 1.57 \pm 0.01$
5	$\frac{\gamma}{\nu} = 1.570 \pm 0.002$	$\frac{\gamma}{\nu} = 1.599 \pm 0.007$
10	$\frac{\gamma}{\nu} = 1.515 \pm 0.003$	$\frac{\gamma}{\nu} = 1.497 \pm 0.006$

8 Discussion and Conclusion

In the discussion, the criteria for the classification of phase transitions introduced in section (4), are compared to the data obtained. Based on these findings, the usability of these criteria in a random geometry setting will be judged. The Potts model coupled to a triangulation is known to have a continuous phase transition for $q \leq 4$ and believed to have a discontinuous transition for higher values of q [2].

Binders cumulant $\mathscr{B}_A$

The Binder cumulant for $q = 2$ and $q = 3$ does not develop a clear minimum, which is in line with the expected continuous phase transition. For $q = 4$, it is not clear whether there is a minimum or not, as after $T = 3$, there were no narrowly spaced measurements taken. Expecting, however that the minimum lays in a region close to the intersection point, it seems unlikely that a minimum is found around $T = 3$. Nevertheless, the data at hand does not allow a conclusion about the order of the phase transition.

For $q = 5$ and $q = 10$, it seems as if a clear minimum develops, which becomes deeper with increasing system size. For both values of q, the minimum develops after exceeding a critical system size. So is the minimum for $q = 5$ approximately visible for $N > 8000$, and for $q = 10$ for $N > 4000$. The occurrence of the minima for $q = 5$ and $q = 10$ indicates the expected discontinuous character of the phase transition.

For all values of q, Binders cumulant fluctuates much. More measurements have to be taken to obtain a smooth graph and definite conclusions about the validity of the criterion to classify the order of the phase transition.

Minimum of the Keutosis U_4

The U_4 criterion for the classification of phase transition states that for a continuous phase transition, the minimum of U_4 should be greater than one. Looking at the absolute minima of U_4 reported in table (7), it can be observed that for $q \leq 4$ the criterion predicts the expected continuous phase transition. For higher values of q, the absolute minima of U_4 are larger than one, and the criterion predicts a continuous phase transition instead of a discontinuous.

Critical exponent ν

The criterion for the critical exponent ν expects a value for ν significant different from one for a continuous phase transition. Comparing to the found values for ν reported in table (8), the criterion has been met for $q \leq 4$, but has not been met for higher values of q.

Conclusion

Both the U_4 and exponent criteria for the classification of phase transitions have been met for $q \leq 4$. However, for $q < 4$ both criteria have not been met. The evidence is not significant enough to conclude a violation of the criteria. Both, the location of the quasi critical temperature and the minimum of U_4 are affected by the finite size of up to $N = 32000$ triangles. To obtain more significance, larger systems need to be considered.

Obtaining ten thousand uncorrelated measurements of the magnetisation for $N = 32000$ triangles has taken approximately between four and eight hours per temperature. To obtain an accurate fit, measurements have been taken in steps of $\Delta T = 0.2$ in the vicinity of minima and maxima of U_4 and the susceptibility respectively. Increasing the system size even more to judge whether the criteria may be met for larger systems, comes at the cost of requiring significantly more computation time. Thus, the criteria do not proof useful, if a quick determination of the order of the phase transition is required

To estimate the exponent ν, the simulation of a larger range of system sizes is needed to obtain the quasi critical temperature as a function of the volume. The criterion involving U_4 may however, be evaluated much faster, as simulations of only one or two large system would be required for an estimate.

About the minimum of Binders cumulant no clear conclusions can be made, because accurate data is missing, especially for $q \leq 4$. The results obtained within this thesis do however seem promising. A minimum seems to develop for $q > 4$, and the discontinuous character of the phase transition is indicated for $q = 5$ and $q = 10$. This is the only one of the three considered criteria, where the discontinuous character is indicated with the obtained data. Therefore, improving the data by adding more measurements near the region of a (possible) minimum is recommended for future research, to rule out the possible emergence of a minimum for $q \leq 4$ and thereby confirm the classification of the phase transition for the q states Potts model.

9 Acknowledgements

I would like to thank Timothy Budd for his excellence mentoring in times of COVID 19. Although all our meetings haven been online, he managed to guide me though the programming, data analysis and writing process by fast, clear and concise answers on my emails and questions. Additionally, he provided me with relevant sources and constructive feedback on all of my work.

Thank you to Ronald Kleiss, who agreed, despite his recent retirement, to act as a second supervisor for the grading of my thesis.

I would like to thank all people involved in the disciplinary honours programme of the faculty of science; the board and all my peers. Being part of this programme allowed me to extend my bachelor internship from 12*E*C to 24EC, and even if I had not the possibility to a foreign visit, this extension made my internship an extra rewarding and educational experience.

A special thank you goes to my peer student from the honours programme Robert Koprinkov, who was almost 24/7 available to answer my questions about C++ error messages. Without him, I would probably have not been able to learn a new programming language so fast and apply it to tackle a scientific problem.

Thank you to Djamel van der Sluis, who was my peer when it comes to doing an internship supervised by Timothy. He especially helped me getting familiar with using the faculties cluster nodes to run code and reminded me of upcoming group meetings.

Last but not least, thank you to Thomas van Poppel for emotional support and warm meals in the week before the deadline. Thank you to my family, who makes it, trough their hard work, possible for me to study in the Netherlands.

A Appendix

A.1 Equilibration

For all equilibration measurements, the magnetisation has been calculated every 10 time steps.

Equilibration for $q = 3$

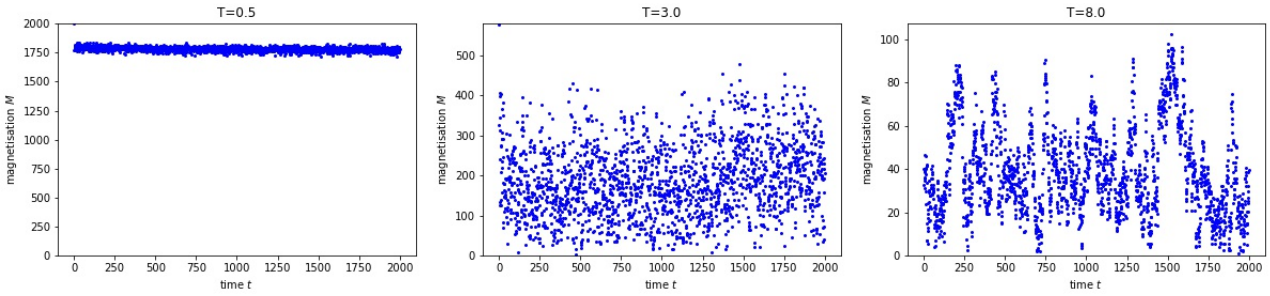

(a) *(b)* *(c)*

Figure 26: Equilibration of the absolute value of the magnetisation vs time of the $q = 3$ states Potts model.

Equilibration for $q = 4$

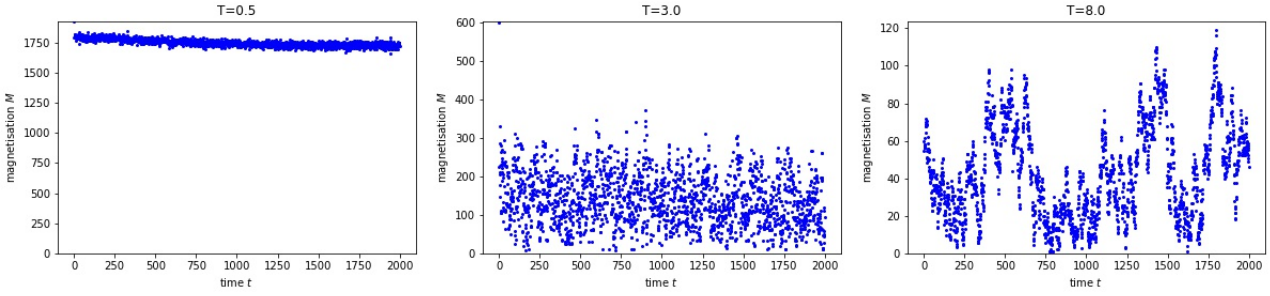

(a) *(b)* *(c)*

Figure 27: Equilibration of the absolute value of the magnetisation vs time of the $q = 4$ states Potts model.

Equilibration for $q = 5$

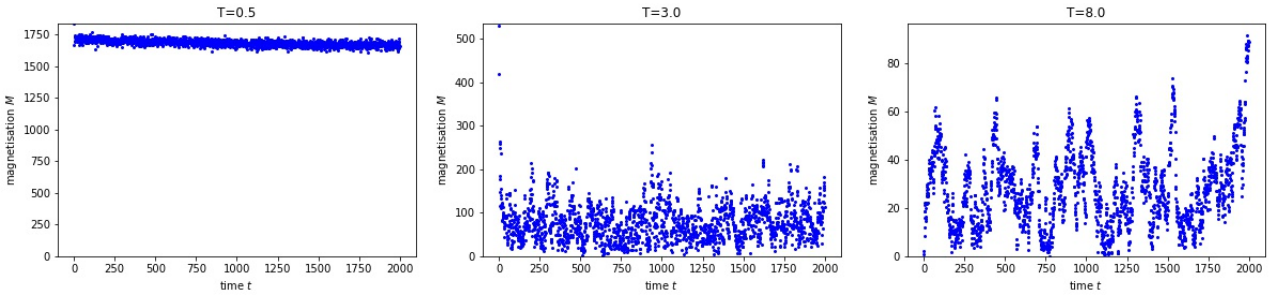

(a) *(b)* *(c)*

Figure 28: Equilibration of the absolute value of the magnetisation vs time of the $q = 5$ *states Potts model.*

Equilibration for $q = 10$

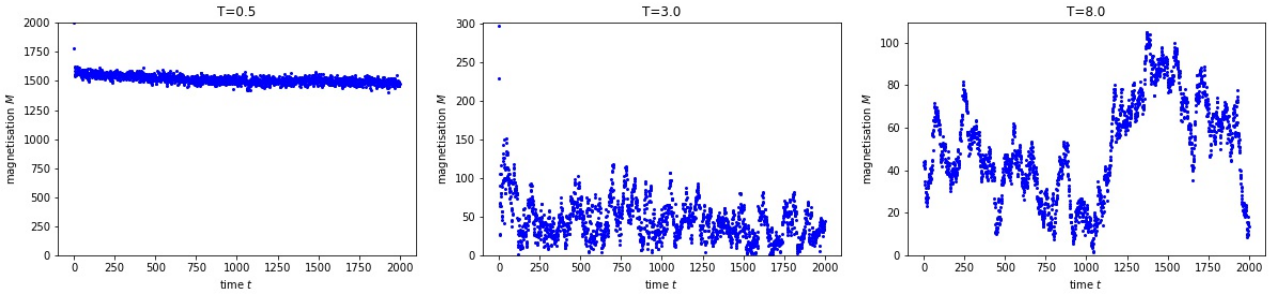

(a) *(b)* *(c)*

Figure 29: Equilibration of the absolute value of the magnetisation vs time of the $q = 10$ *states Potts model.*

A.2 Magnetisation autocorrelation time

Measurements of the magnetisation were taken every ten sweeps. The equilibration time was 500 sweeps.

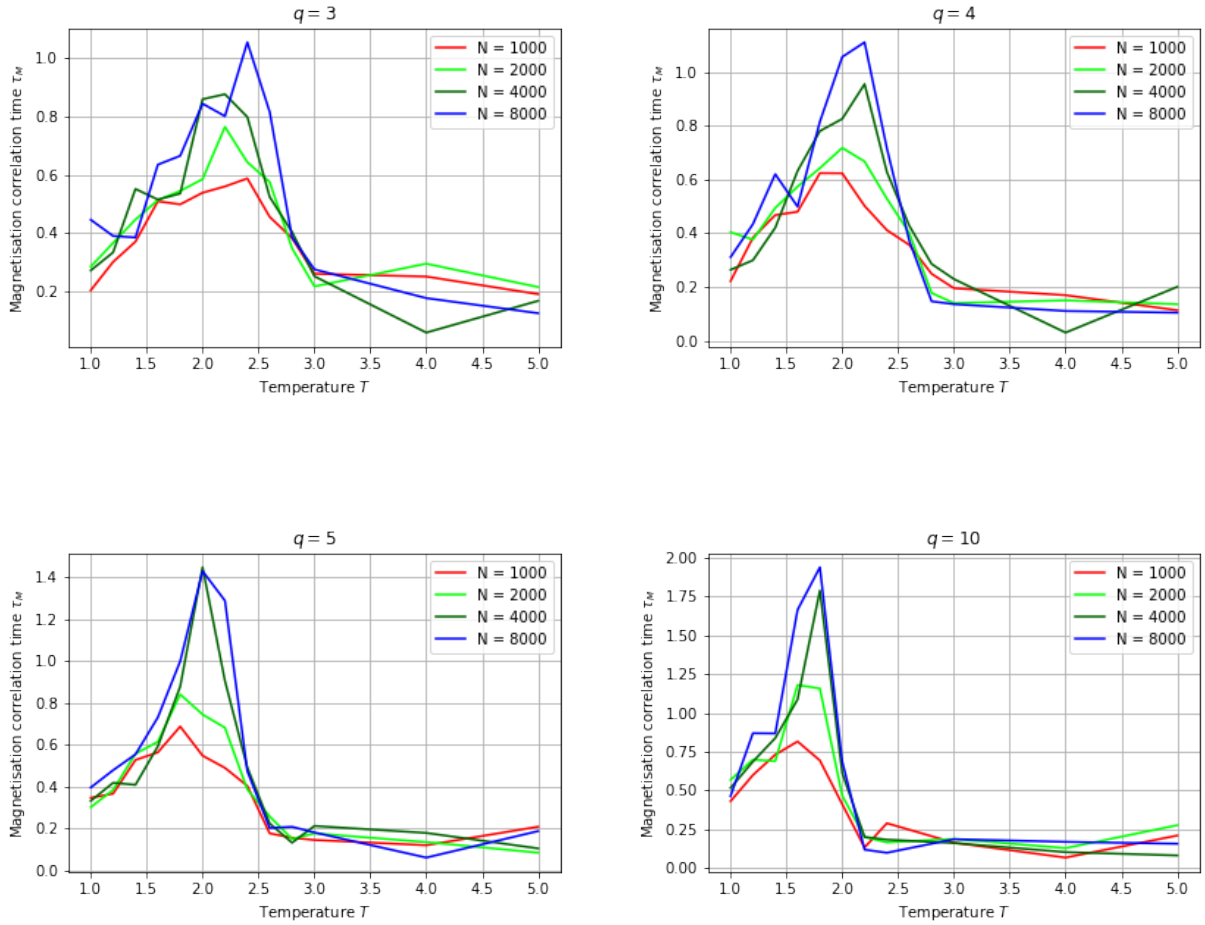

Figure 31: Magnetisation autocorrelation time in time steps of ten sweeps of the $q = 3,4,5,10$ states Potts model coupled to a dynamical triangulation for $N = 1000,2000,4000,8000$ triangles.

A.3 Magnetisation

The following graphs show the magnetisation vs temperature for the $q = 3, 4, 5, 10$ state Potts model. The magnetisation is normalised by dividing through the maximal magnetisation for the given system size. That corresponds to the value of the magnetisation at the first measured temperature. Theoretically, the magnetisation is maximal for $T = 0$.

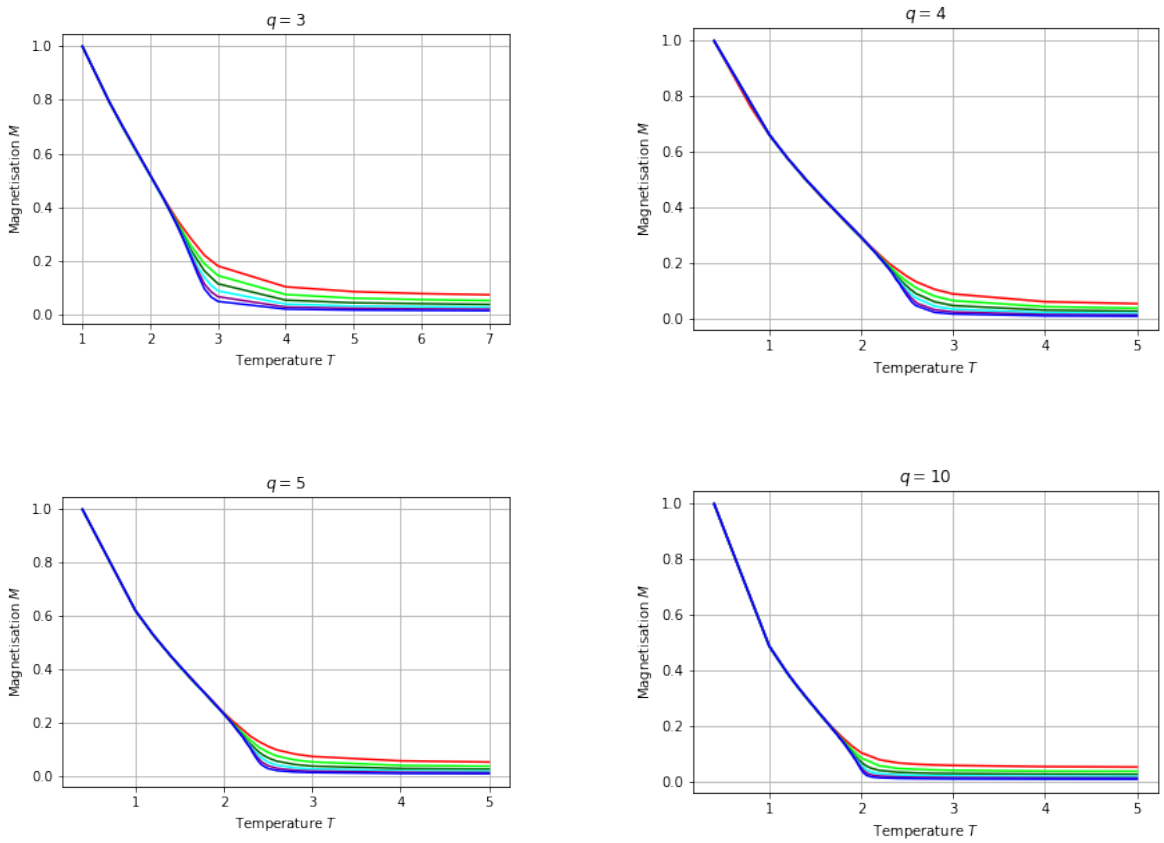

Figure 33: Magnetisation of the $q = 3, 4, 5, 10$ states Potts model coupled to a dynamical triangulation.

A.4 Magnetic susceptibility

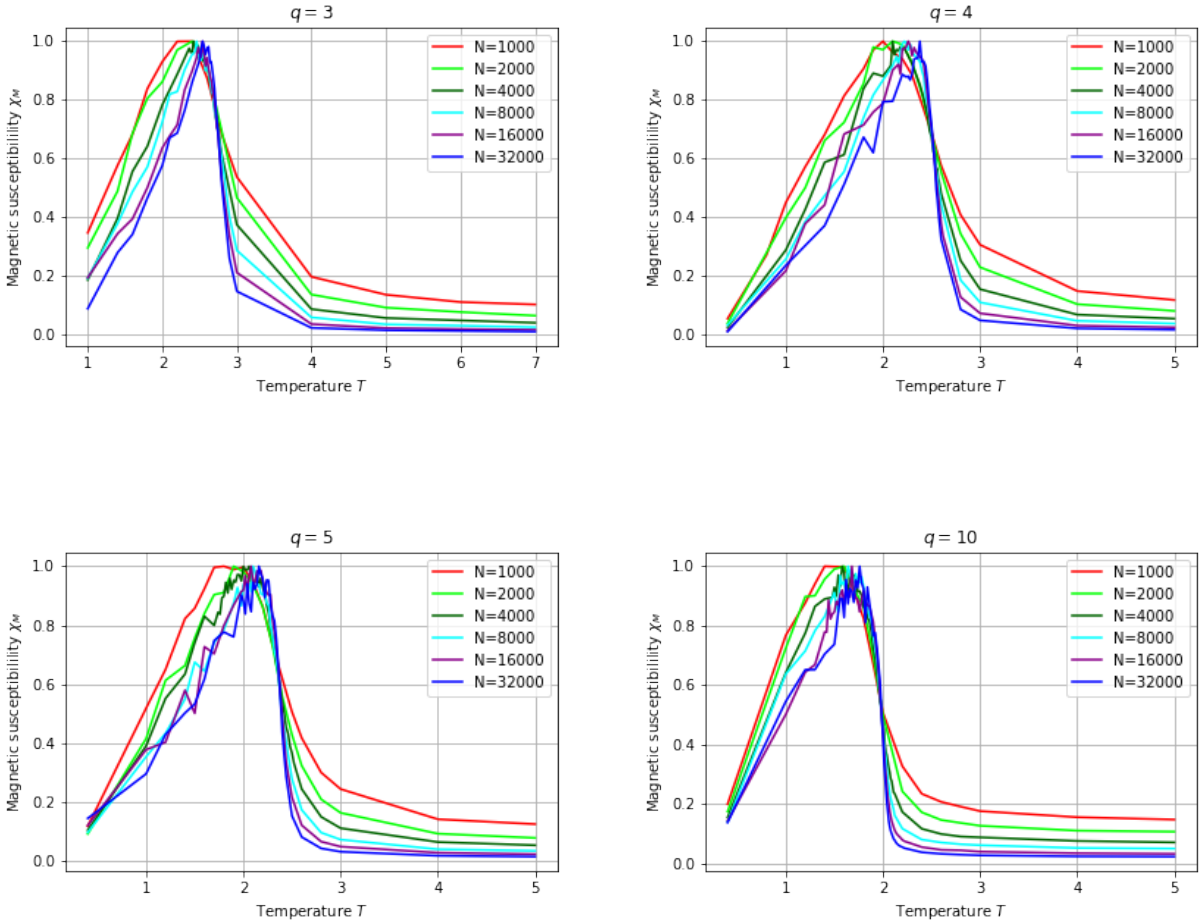

Figure 35: Magnetic susceptibility of the $q = 3,4,5,10$ states Potts model coupled to dynamical triangulations as a function of temperature for $N = 1000,2000,4000,8000,16000,32000$ triangles. The susceptibility is re-scaled by its respective maximal value for each system size. The rapid fluctuations near the maximum are caused by adding more measurements per temperature interval.

A.5 Scaling of the quasi critical temperature

The following plots show the quasi critical temperature as a function of the volume determined from the maximum of the magnetic susceptibility with a polynomial fit and an univariant spline. The error is determined by performing 70 resamplings.

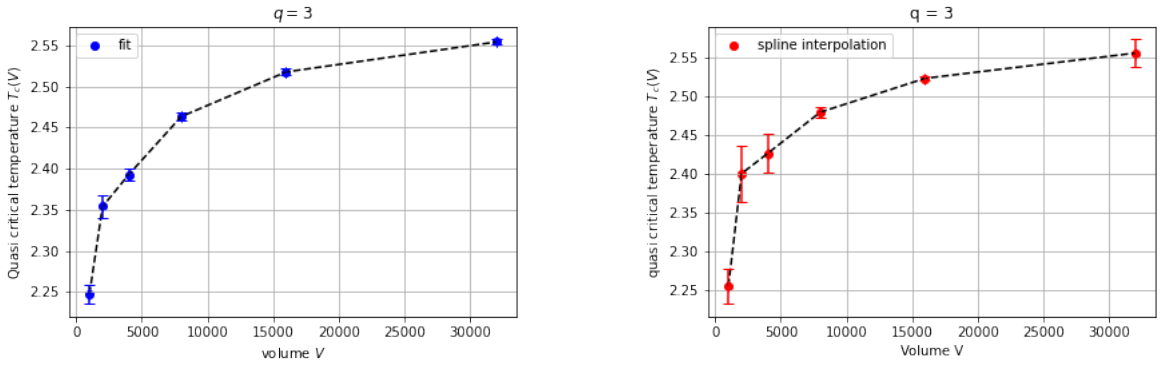

(a) *(b)*

Figure 36: (a) polynomial fit with degree $[8,10,10,12,12,12]$ *and (b) univariant spline with smoothing factor* $[5\cdot10^3, 5\cdot10^4, 0.5\cdot10^6, 7\cdot10^7, 5\cdot10^8, 1\cdot10^9]$

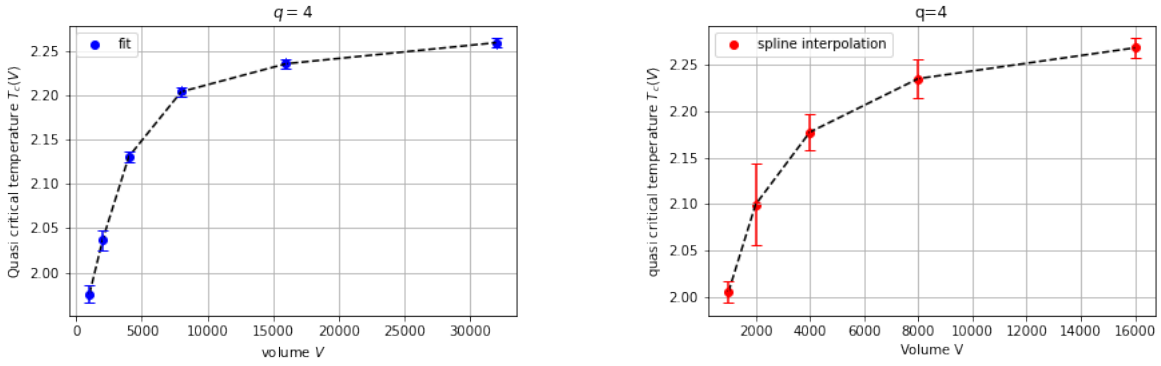

(a) *(b)*

Figure 37: (a) polynomial fit with degree $[6,6,8,10,10,10]$ *and (b) univariant spline with smoothing factor* $[1\cdot10^2, 5\cdot10^4, 2\cdot10^6, 1\cdot10^7, 6\cdot10^8, 7\cdot10^8]$

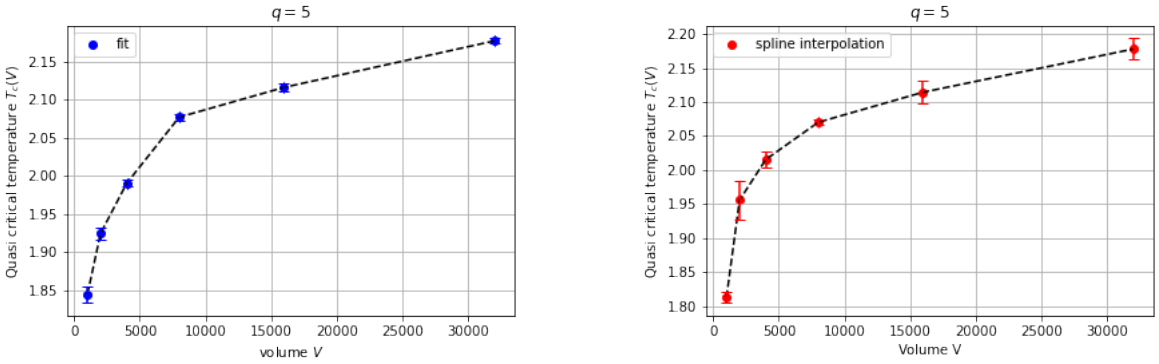

(a) *(b)*

Figure 38: (a) polynomial fit with degree $[8,8,8,10,12,14]$ *and (b) univariant spline with smoothing factor* $[5\cdot10^4, 5\cdot10^4, 7\cdot10^6, 10\cdot10^7, 8\cdot10^8, 3\cdot10^9]$

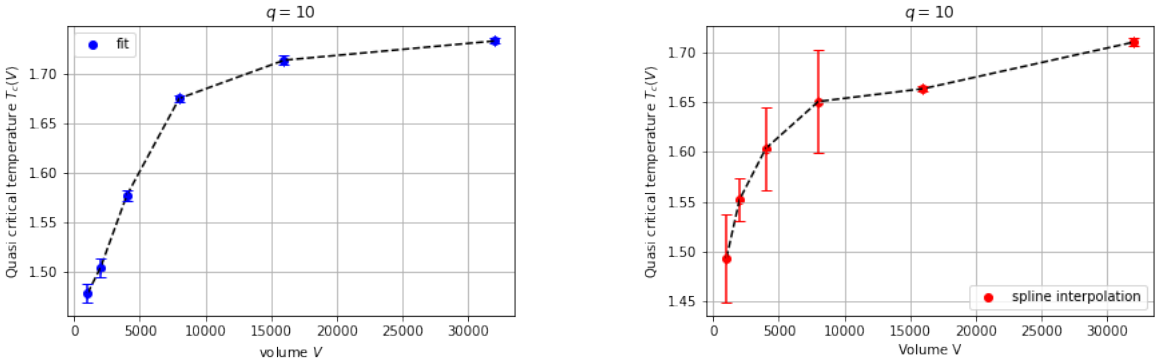

(a) *(b)*

Figure 39: (a) polynomial fit with degree $[8,8,8,10,12,12]$ *and (b) univariant spline with smoothing factor* $[1\cdot10^3, 3\cdot10^4, 9\cdot10^5, 5\cdot10^6, 1\cdot10^9, 1,4\cdot10^10]$

A.6 Scaling of the magnetic susceptibility

The following plots show the scaling of the magnetic susceptibility as a function of the volume. The maximum of the magnetic susceptibility is in each case determined with a fit (a) and an univariant spline interpolation (b), where the fitting parameters indicated in appendix (A.5) are used.

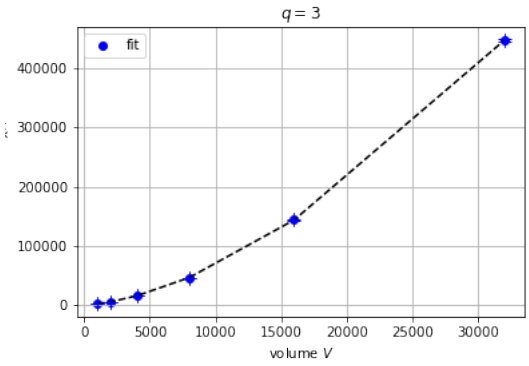

(a)

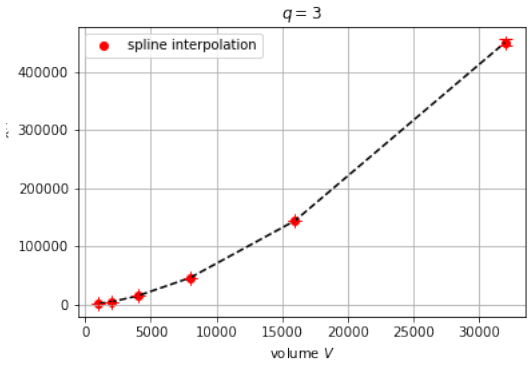

(b)

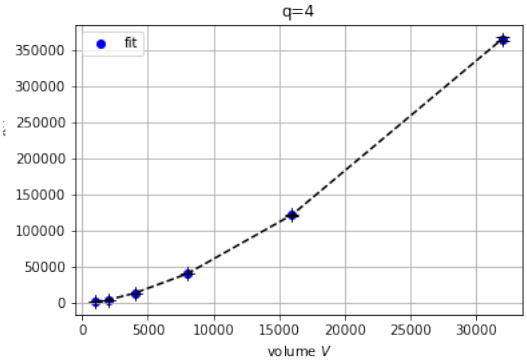

(a)

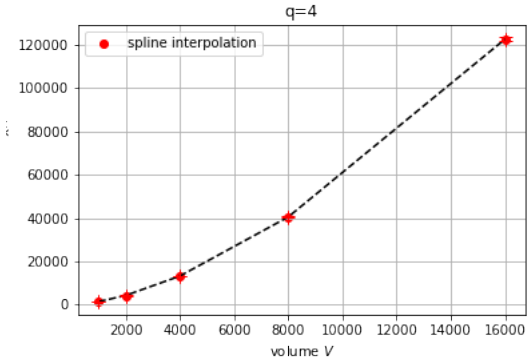

(b)

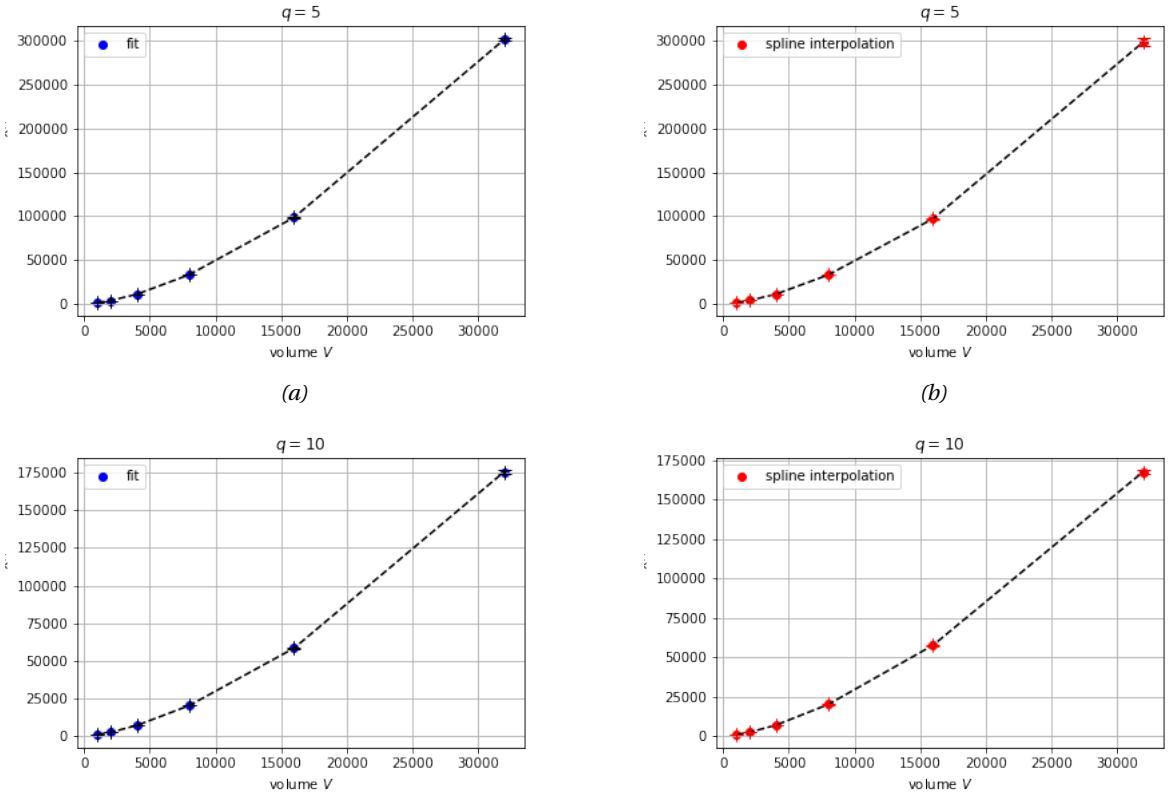

Figure 42: Scaling of the magnetic susceptibility for $q = 3, 4, 5, 10$.

A.7 The Keutosis U_4

The tables below summarise the results of the fit and interpolation analysis of the minimum of the Keutosis U_4 of the magnetisation. The error is in each case determined by performing 70 resamplings with the Bootstrap method.

q=3:

Table 10: $q = 3$, *fitting degree* $[4,4,4,8,8,8]$, *smoothing factor* $[0.01, 0.05, 0.05, 0.05, 0.05, 0.05]$

N	fit	interpolation	fit	interpolation
1000	$T_c = 2.62 \pm 0.06$	$T_c = 2.52 \pm 0.03$	$\min(U_4) = 2.53 \pm 0.03$	$\min(U_4) = 2.51 \pm 0.04$
2000	$T_c = 2.71 \pm 0.02$	$T_c = 2.61 \pm 0.04$	$\min(U_4) = 2.38 \pm 0.04$	$\min(U_4) = 2.44 \pm 0.05$
4000	$T_c = 2.68 \pm 0.02$	$T_c = 2.64 \pm 0.05$	$\min(U_4) = 2.44 \pm 0.02$	$\min(U_4) = 2.40 \pm 0.07$
8000	$T_c = 2.68 \pm 0.02$	$T_c = 2.66 \pm 0.02$	$\min(U_4) = 2.432 \pm 0.009$	$\min(U_4) = 2.40 \pm 0.02$
16000	$T_c = 2.684 \pm 0.009$	$T_c = 2.66 \pm 0.09$	$\min(U_4) = 2.39 \pm 0.01$	$\min(U_4) = 2.38 \pm 0.07$
32000	$T_c = 2.70 \pm 0.01$	$T_c = 2.70 \pm 0.01$	$\min(U_4) = 2.42 \pm 0.02$	$\min(U_4) = 2.38 \pm 0.01$

q=4:

Table 11: $q = 4$, *fitting degree* $[6,6,6,8,8,8]$, *smoothing factor* $[0.3, 0.3, 0.1, 0.3, 0.1, 0.2]$

N	fit	interpolation	fit	interpolation
1000	$T_c = 2.40 \pm 0.02$	$T_c = 2.46 \pm 0.02$	$\min(U_4) = 2.42 \pm 0.01$	$\min(U_4) = 2.44 \pm 0.03$
2000	$T_c = 2.44 \pm 0.02$	$T_c = 2.50 \pm 0.03$	$\min(U_4) = 2.43 \pm 0.02$	$\min(U_4) = 2.44 \pm 0.05$
4000	$T_c = 2.464 \pm 0.008$	$T_c = 2.463 \pm 0.004$	$\min(U_4) = 2.389 \pm 0.009$	$\min(U_4) = 2.38 \pm 0.01$
8000	$T_c = 2.49 \pm 0.04$	$T_c = 2.478 \pm 0.004$	$\min(U_4) = 2.4 \pm 0.1$	$\min(U_4) = 2.37 \pm 0.03$
16000	$T_c = 2.49 \pm 0.02$	$T_c = 2.489 \pm 0.006$	$\min(U_4) = 2.38 \pm 0.09$	$\min(U_4) = 2.37 \pm 0.02$
32000	$T_c = 2.493 \pm 0.002$	$T_c = 2.49 \pm 0.04$	$\min(U_4) = 2.40 \pm 0.02$	$\min(U_4) = 2.37 \pm 0.05$

q=5:

Table 12: $q = 5$, *fitting degree* $[4,8,8,10,10,12]$, *smoothing factor* $[0.08,0.08,0.3,0.3,0.3,0.5]$

N	fit	interpolation	fit	interpolation
1000	$T_c = 2.23 \pm 0.01$	$T_c = 2.19 \pm 0.03$	$\min(U_4) = 2.47 \pm 0.02$	$\min(U_4) = 2.47 \pm 0.03$
2000	$T_c = 2.25 \pm 0.06$	$T_c = 2.25 \pm 0.02$	$\min(U_4) = 2.5 \pm 0.1$	$\min(U_4) = 2.45 \pm 0.03$
4000	$T_c = 2.29 \pm 0.08$	$T_c = 2.28 \pm 0.01$	$\min(U_4) = 2.4 \pm 0.1$	$\min(U_4) = 2.37 \pm 0.02$
8000	$T_c = 2.32 \pm 0.04$	$T_c = 2.305 \pm 0.005$	$\min(U_4) = 2.4 \pm 0.1$	$\min(U_4) = 2.36 \pm 0.03$
16000	$T_c = 2.32 \pm 0.09$	$T_c = 2.322 \pm 0.004$	$\min(U_4) = 2.6 \pm 0.27$	$\min(U_4) = 2.39 \pm 0.03$
32000	$T_c = 2.3 \pm 0.2$	$T_c = 2.339 \pm 0.007$	$\min(U_4) = 4 \pm 3$	$\min(U_4) = 2.36 \pm 0.05$

q=10:

Table 13: $q = 10$, *fitting degree* $[6,8,8,10,10,12]$, *smoothing factor* $[0.01,0.01,0.05,0.02,0.03,0.6]$

N	fit	interpolation	fit	interpolation
1000	$T_c = 1.783 \pm 0.008$	$T_c = 1.80 \pm 0.02$	$\min(U_4) = 2.51 \pm 0.02$	$\min(U_4) = 2.48 \pm 0.03$
2000	$T_c = 1.84 \pm 0.01$	$T_c = 1.86 \pm 0.01$	$\min(U_4) = 2.51 \pm 0.03$	$\min(U_4) = 2.47 \pm 0.04$
4000	$T_c = 1.874 \pm 0.002$	$T_c = 1.9 \pm 0.2$	$\min(U_4) = 2.51 \pm 0.01$	$\min(U_4) = 2.3 \pm 0.3$
8000	$T_c = 1.908 \pm 0.003$	$T_c = 2.0 \pm 0.1$	$\min(U_4) = 2.48 \pm 0.02$	$\min(U_4) = 3 \pm 1$
16000	$T_c = 1.942 \pm 0.006$	$T_c = 2.0 \pm 0.2$	$\min(U_4) = 2.67 \pm 0.05$	$\min(U_4) = 2.4 \pm 0.2$
32000	$T_c = 1.9 \pm 0.1$	$T_c = 1.967 \pm 0.005$	$\min(U_4) = 4 \pm 2$	$\min(U_4) = 2.42 \pm 0.03$

A.8 Histograms

The following section includes histograms of the magnetisation and the magnetisation polar angle for $q = 10$. These give insight into the occupation probability of a given state of the system. It shows nicely, how increasing the temperature influences this distribution.

Magnetisation histogram

The darker the grey scale, the larger the system size. It can be seen that the width of the peak decreases with increasing system size, meaning that the finite size effects become smaller. Also, fluctuations are the largest close to the quasi critical temperature.

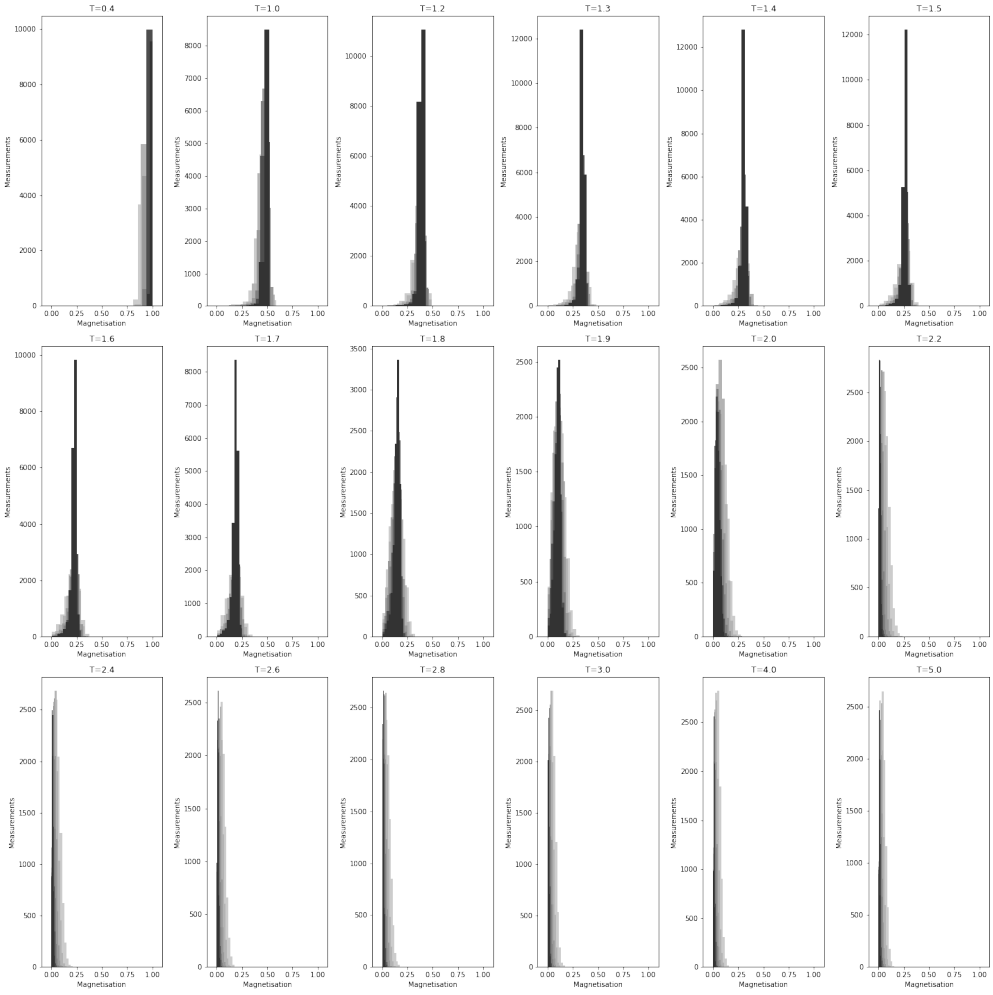

Figure 43: Magnetisation histogram for $q = 10$.

Polarangle histogram

The polarangle is plotted as a function of time for each temperature. Increasing system sizes are again indicated by a darker colour. Larger system sizes maintain the structure of the ground states longer, and transition at a higher quasi critical temperature.

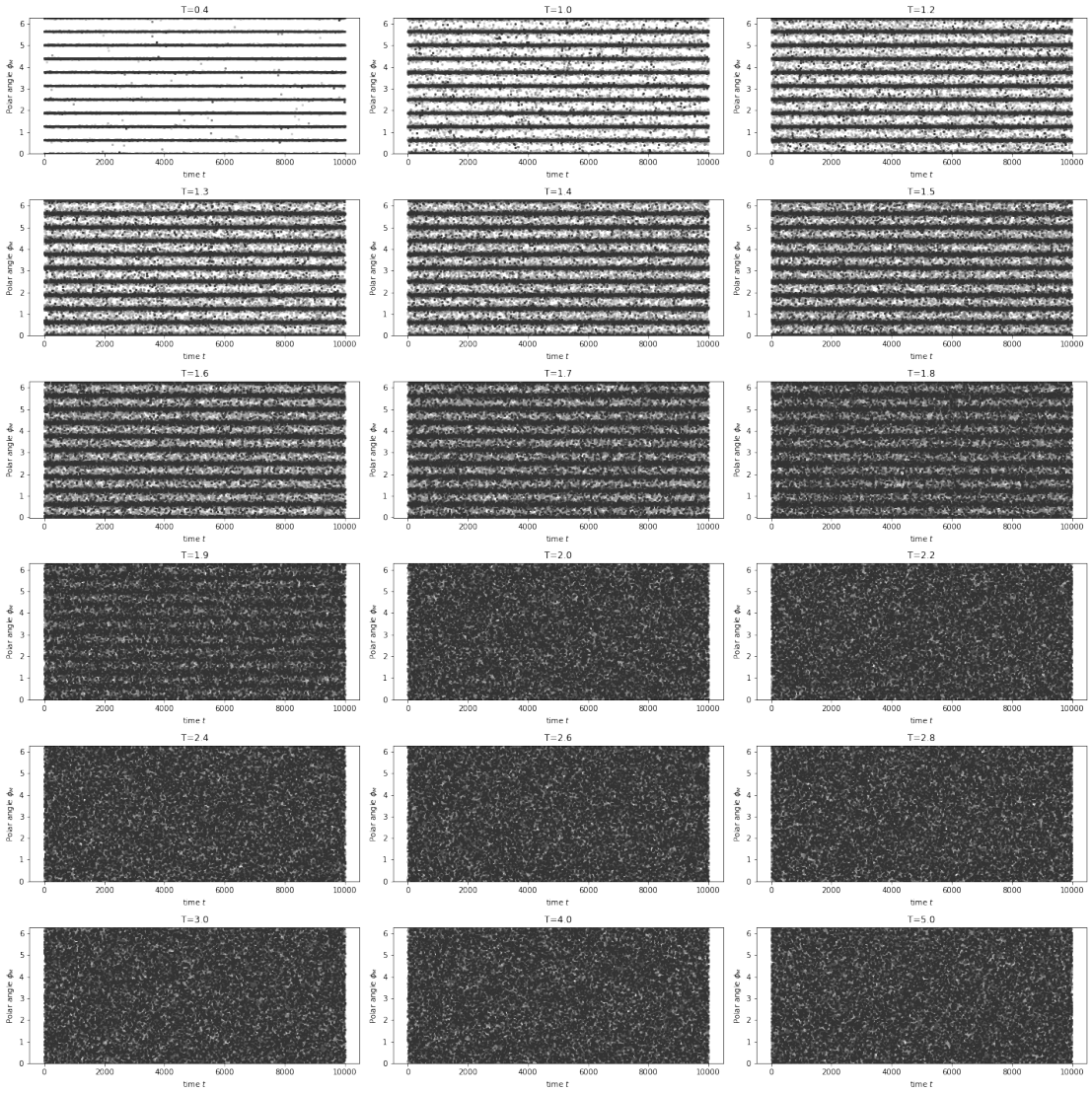

Figure 44: Polar angle histogram for $q = 10$.

References

[1] R. Loll, "The Emergence of Spacetime," pp. 1–22.

[2] B. Eynard and G. Bonnet, "The Potts-q random matrix model: Loop equations, critical exponents, and rational case," *Physics Letters, Section B: Nuclear, Elementary Particle and High-Energy Physics*, vol. 463, no. 2-4, pp. 273–279, 1999.

[3] D. Benedetti, "Quantum Gravity from Simplices : Analytical Investigations of Causal Dynamical Triangulations arXiv : 0707 . 3070v1 [gr-qc] 20 Jul 2007," no. Chapter 1.

[4] D. Ashton, "Scale invariance in the critical ising model." `https://www.youtube.com/watch?v=fi-g2ET97W8`.

[5] J. M. Yeomans, "Statistical Mechanics of Phase Transitions," *Oxford University Press*, pp. 1–300, 1992.

[6] S. Jordan, J. Jurkiewicz, and R. Loll, "Second- and First-Order Phase Transitions in CDT," pp. 1–24.

[7] M. E. J. Newman and G. T. Barkema, "Monte Carlo Methods in Statistical Physics," *Oxford University Press*, pp. 1–300, 1999.

[8] C. Perot, "Simulating magnetism part 4: The q -state potts model." https://cameronperot.com/physics/2020/05/14/simulating-magnetism-part-4.html.

[9] T. Budd, "Monte Carlo methods in Dynamical Triangulations Part I : 2D random geometry, https://hef.ru.nl/ tbudd/randgeom/," 2017.

[10] Picture, "Delaunay triangulation." https://en.wikipedia.org/wiki/File:Delaunay_Triangulation_(25_Points).svg.

[11] P. D. B. R. K Pathria, *Statistical mechancis*. 2011.

[12] B. Krüger, *Simulating Triangulations: Graphs, Manifolds and (Quantum) Spacetime*.

[13] Kojevnikov, Alexei, "Paul ehrenfest." https://www.britannica.com/biography/Paul-Ehrenfest.

[14] K. Binder, *Monte Carlo methods in statistical physics 2nd ed.* Topics in Current Physics, 7. Berlin: Springer-Verlag, 1996.

[15] K. Eichhorn and K. Binder, "Reports on Progress in Physics Related content Applications of Monte Carlo methods to statistical physics," 1997.

[16] K. Vollmayr, J. D. Reger, M. Schencher, K. Binder, I. Physik, J. Gutenberg, S. Weg, and W. Mainz, "Finite size effects at thermally-driven first order phase transitions : a phenomenological theory of the order parameter distribution," vol. 125, pp. 113–125, 1993.

[17] H. Meyer-Ortmanns, "Phase transitions in quantum chromodynamcis," *Physical Review B - Condensed Matter and Materials Physics*, vol. 54, no. 20, pp. 14532–14539, 1996.

[18] J. Ambjørn, S. Jordan, J. Jurkiewicz, and R. Loll, "Second- and first-order phase transitions in causal dynamical triangulations," *Physical Review D - Particles, Fields, Gravitation and Cosmology*, vol. 85, no. 12, pp. 1–10, 2012.

[19] E. A. Guggenheim, "The principle of corresponding states," *The Journal of Chemical Physics*, vol. 13, no. 7, pp. 253–261, 1945.